



# Microseismicity-based method for the dynamic estimation of the potential rockburst scale during tunnel excavation

Guo-Feng Liu<sup>1,2</sup> · Quan Jiang<sup>2</sup> · Guang-Liang Feng<sup>2</sup> · Dong-Fang Chen<sup>3</sup> · Bing-Rui Chen<sup>2</sup> · Zhou-Neng Zhao<sup>4</sup>

Received: 17 February 2020 / Accepted: 2 March 2021 / Published online: 11 March 2021  
© Springer-Verlag GmbH Germany, part of Springer Nature 2021

## Abstract

The severity and harmfulness of a rockburst event are significantly correlated with the scale of rock mass ejection, especially when the rock mass are not supported. This paper presents a microseismicity-based method for the early estimation of rockburst occurrence and its potential scale, which is graded according to the volume of the rockburst pit ( $R_v$ ). The establishment of the estimation method involves a rockburst database, a grading scheme of the rockburst scale, selection and clustering analysis of rockburst samples, training of an artificial neural network (ANN) model, and dynamic updating. Firstly, a rockburst database is established from cases that were collected from the tunnels at depths of 1900–2525 m in the Jinping II hydropower station, located in southwest China. A grading scheme regarding the rockburst scale is preliminarily proposed on the basis of statistical analysis. Next, seventy-four rockburst cases, collected in tunnels with microseismic (MS) monitoring from October 2010 to March 2011, are selected as typical rockburst samples by using cluster analysis, and the relationships between the microseismicity and rockburst scale are deeply revealed. Then, three MS parameters, namely, the cumulative number of events, the cumulative energy, and the cumulative apparent volume, are determined and used together as input indicators for the identification of the rockburst scale. The estimation model is trained and cross-validated by the ANN optimized through genetic algorithm (GA). Finally, the performance of this microseismicity-based method has been validated by thirty-one cases that occurred in the tunnels with a cumulative length of 1.85 km, excavated from April 2011 to November 2011. The result indicates that approximately 83.9% of the rockburst cases could be reliably estimated. This study provides a new and feasible method for rockburst scale estimation, which can be used separately or applied as a complementary approach to current prediction methods for risk assessment and management of rockbursts in drill-and-blast tunneling.

**Keywords** Rockburst scale · Microseismicity · Neural network model · Risk estimation · Deep tunnel

## Introduction

With the rapid development and utilization of the deep underground space, an increasing amount of rock fracturing phenomena and associated rockburst hazards have emerged

surrounding the excavation of highly stressed rock masses in deep underground engineering. The rockburst is a sudden release of elastic energy that has accumulated in rock masses under tunnel excavation or other disturbances. It can result in the violent failure and ejection of surrounding rock (Ortlepp and Stacey 1994; Kaiser et al. 1996; Gong et al. 2019) and often causes various undesirable consequences in engineering construction (Liu et al. 2016; Wang et al. 2019; Chinese standards 2019). Overall, the harmfulness of a rockburst, which includes the series of consequences and losses, is significantly correlated with the scale of the surrounding rock ejection. The rockburst intensity (none, slight, moderate, intense, or extremely intense) has been used as a common index to describe the severity of a rockburst. The maximum failure depth of the rockburst pit is always used as one of the most important evaluation factors to describe the characteristic and determine the intensity of a rockburst (Kaiser et al. 1996;

✉ Quan Jiang  
qjiang@whrsm.ac.cn

<sup>1</sup> School of Highway, Chang'an University, Xi'an 710064, China

<sup>2</sup> State Key Laboratory of Geomechanics and Geotechnical Engineering, Institute of Rock and Soil Mechanics, Chinese Academy of Sciences, Wuhan 430071, China

<sup>3</sup> School of Resources and Environmental Engineering, Wuhan University of Technology, Wuhan 430071, China

<sup>4</sup> School of Environment and Resource, Southwest University of Science and Technology, Mianyang 621010, China

Chinese standards 2016). The depth of a rockburst is easily obtainable in engineering practice, and it can reflect the rockburst scale to some extent. However, two rockbursts with approximately the same failure depth or the same intensity may differ in terms of the scale of rock mass ejection. Alternatively, the volume of the rockburst pit ( $R_v$ ) could be adopted to describe the rockburst scale from the three-dimensional perspective. The larger the  $R_v$  is, the larger the amount of failed rock a rockburst generates.

The prediction and warning of rockburst risk have constituted a global problem in deep tunneling and mining engineering. Over the past few decades, microseismic (MS) monitoring techniques that involve three-dimensional monitoring of micro-cracking events in rocks have been frequently applied for monitoring rockburst risk for their advantages of continuity, real-time performance, and precision in tracking the development process of macroscopic rock failure behaviors. MS waves released from rock cracking can be captured by using sensors that are positioned at various azimuths. Then, the time, location, energy, and type of rock cracks can be gradually obtained as precursor information of a rockburst, based on which, an early prediction of impending rockburst risk may be conducted. The technology was initially applied in deep mines (McCreary et al. 1992; Mendecki 1996) for the management of rockburst monitoring. Aswegen and Bulter (1993) presented the application of quantitative seismology to mining safety in South African gold mines. Afterward, studies regarding the MS monitoring of rockbursts in underground tunnels were conducted. MS data contain an enormous amount of information about the rock mechanics and have been well used to elucidate the rocks' mechanical properties (Cai et al. 2001). The technology has been widely applied in deep tunnel engineering for the research and management of rockburst monitoring. Several advantageous techniques for improving MS monitoring in long, deep tunnels were developed by Feng et al. (2013) and Feng (2017). The analysis on the evolution properties of important MS parameters, such as MS events, apparent volume, energy index, the  $b$ -value, and so on in the rockburst development process, is commonly used in the prediction of rockburst risk. Ma et al. (2015) proved that the microseismic activities are of temporal priority and spatial consistency with rockburst events through case studies from the deep-buried tunnels in a hydropower station. Feng et al. (2015b) found that the evolution of the cumulative number of MS events, cumulative MS energy, cumulative MS apparent volume, MS event rate, MS energy rate, and MS apparent volume rate affect the rockburst intensity significantly. On the basis, a rockburst warning formula for dynamic warning of rockburst intensity was proposed, and it has been successfully applied in engineering practice. Xu et al. (2016) found that the concentration of MS events before a strainburst is a significant precursor. Yu et al. (2016) suggested that the daily maximum microseismic energy can be used as a basis

for estimating the rockburst based on an analysis of hundreds of rockburst cases. Current researches have shown that rockburst prediction in tunneling mainly focuses on the position, the range of the failure depth, and the intensity according to the precursory MS information during the development process of a rockburst, and various degrees of success have been achieved in plenty engineering practices (Tang et al. 2010; Feng et al. 2012, 2013; Chen et al. 2012; Feng et al. 2015b, 2020; Ma et al. 2015; Xu et al. 2016; Zhang et al. 2018; Hu et al. 2019; Li et al. 2021). The prediction of the exact volume of the ejected rock mass ( $R_v$ ) seems very difficult at present; however, it is of guiding significance in applications if the occurrence and a probable range of the potential scale of a rockburst are early estimated. It would further contribute to rockburst risk assessment and management when the intensity and scale of a potential rockburst are both predictable. However, the relation between the microseismicity and the potential rockburst scale, which are closely interrelated, has long been unexamined in previous researches. And an associated method for the dynamic estimation of the rockburst scale risk has yet to be established.

Based on the deep tunnels with a maximum burial depth of 2525 m in the Jinping II hydropower station, located in southwest China, this paper aims at presenting a new method for the risk estimation of potential rockburst scale. Firstly, a preliminary scheme of grading the rockburst scale by the volume of the rockburst is proposed based on statistical analysis of hundreds of rockburst cases. Then, the relationships between the microseismic information and rockburst scale are revealed through a comprehensive statistical analysis. After that, a new method for utilizing the key MS parameters to estimate rockburst scale is established, based on the use of an artificial neural network (ANN) which is optimized by a genetic algorithm (GA). Finally, the dynamic estimation on the rockburst occurrence and its potential scale in real time during tunnel excavation is clearly presented via a case analysis. In practice, multiple cases in the tunnels with a cumulative length of 1.85 km have been analyzed to validate the applicability of the microseismicity-based method.

## Basic information of project and the rockburst database

### Project profile

The Jinping II hydropower project is located on the Yalong River, in Sichuan Province in southwestern China, as shown in Fig. 1, which has the largest and deepest water tunnel system in the world. The tunnel system consists of four headrace tunnels, two assistant tunnels, and one drainage tunnel at depths of between 1900 and 2525 m. The seven tunnels have the same length of 16.67 km, and they are parallel to each

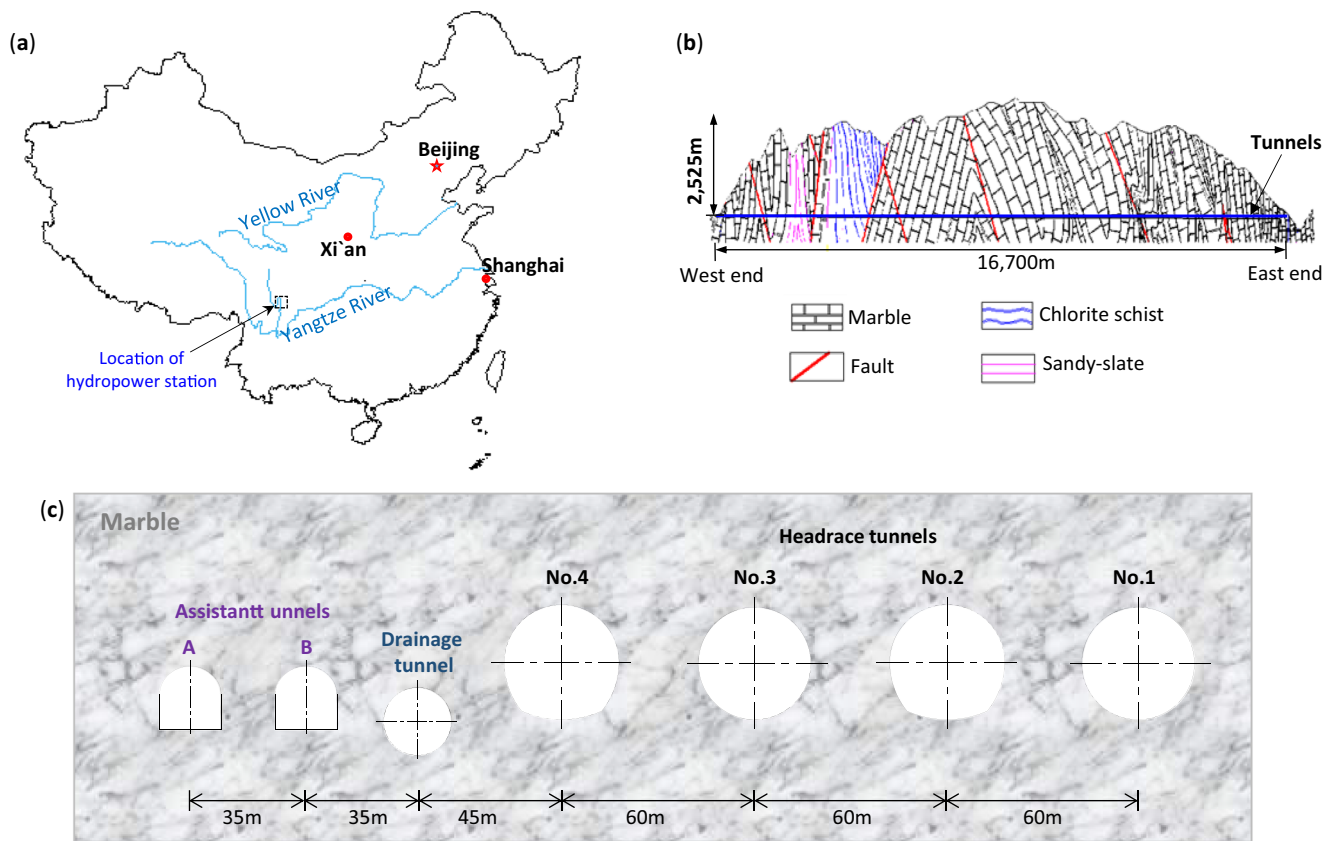


**Fig. 1** Location and general layout of the Jinping II hydropower station: **a** the location of the Jinping project in China, **b** the geological profile along the tunnels, and **c** the layout of the tunnels

other. The headrace tunnels have a circular cross section that is 12.4–13 m in diameter, and the drainage tunnel is 7.2 m in diameter. The stratigraphic rock surrounding the tunnels is mostly marble formation, which belongs to the Triassic system. According to the in situ stress data measured through hydraulic fracturing technique and back analysis of the in situ stress field, the maximum and minimum principal stress on the cross section of the tunnel at the depth of around 2500 m were approximately 69 and 45 MPa, respectively. The maximum principal stress was nearly vertical, and the minimum principle stress was nearly horizontal. According to Chinese “Standard for engineering classification of rock mass” (Feng and Hudson 2011), the quality of rock mass is ranked as “II” and “III,” which are conducive to the construction of underground tunnels. According to the GSI classification (Hoek et al. 1998), the index of rock mass quality is approximately 60–80.

**Mechanical strength of marble**

Laboratory uniaxial compression tests for the marbles collected at the site of the headrace tunnels were performed, and the results indicated that the failure behavior of the marbles is characterized by typical brittle splitting, whose slices were nearly parallel to the axis of the cylinder specimens (see Fig.

2). The uniaxial compression strengths (UCS) of such marbles were mostly 100–140 MPa, and further Brazil disk split tests showed that the indirect tensile strengths (TS) of the marbles were mostly 3–6 MPa. The value of the TS/UCS is distinctly low and the rock mass would be more prone to tensile failure. According to the strength-stress ratio (less than 2) and rock properties, there would be significant rockburst risks during the excavation activities. In fact, rockburst hazards were frequently encountered in the excavation period of these tunnels (Jiang et al. 2010; Feng et al. 2013; Zhang et al. 2013), which resulted in a series of unexpected impacts, as the examples shown in Fig. 3.

**Rockburst database**

According to field investigations on two assistant parallel tunnels that were completed prior to the other five tunnels, 18.5 and 16.3% of the excavated tunnel lengths had been affected by rockbursts (Shan and Yan 2010). Therefore, to reduce the subsequent rockburst risk, a high-performance integrated seismic system (ISS) was adopted for rockburst monitoring in the headrace and drainage tunnels. Details on the MS monitoring network are available in the relevant reference (Feng et al. 2015a).



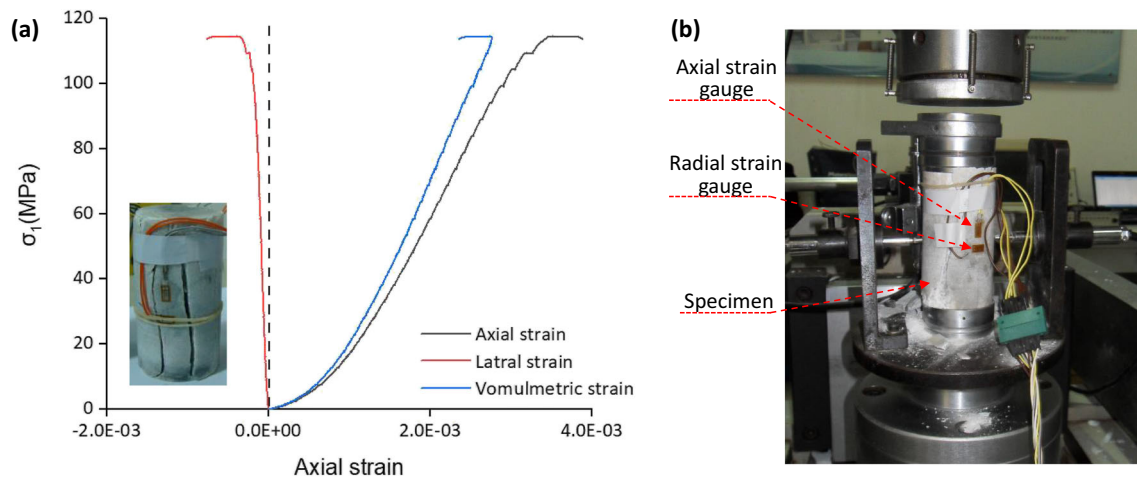


**Fig. 2** Result of the typical uniaxial compression test of marble: **a** the stress-strain curve and **b** measuring method

Firsthand information on rockburst cases is essential for the study of rockburst hazards, which can be well managed by constructing a database. Therefore, a dynamic rockburst database for four headrace tunnels and the drainage tunnel was built from the period of early excavation. The rockburst database became richer as more tunnels were excavated, and the rockbursts that were collected earlier could be analyzed to establish a related estimation or prediction method for

application in subsequent tunnel construction for rockburst risk analysis.

A suitable database of rockburst cases must contain the following rockburst information:

- Rockburst intensity (none, slight, moderate, intense, or extremely intense)
- Spatiotemporal information on the rockburst and related geological conditions

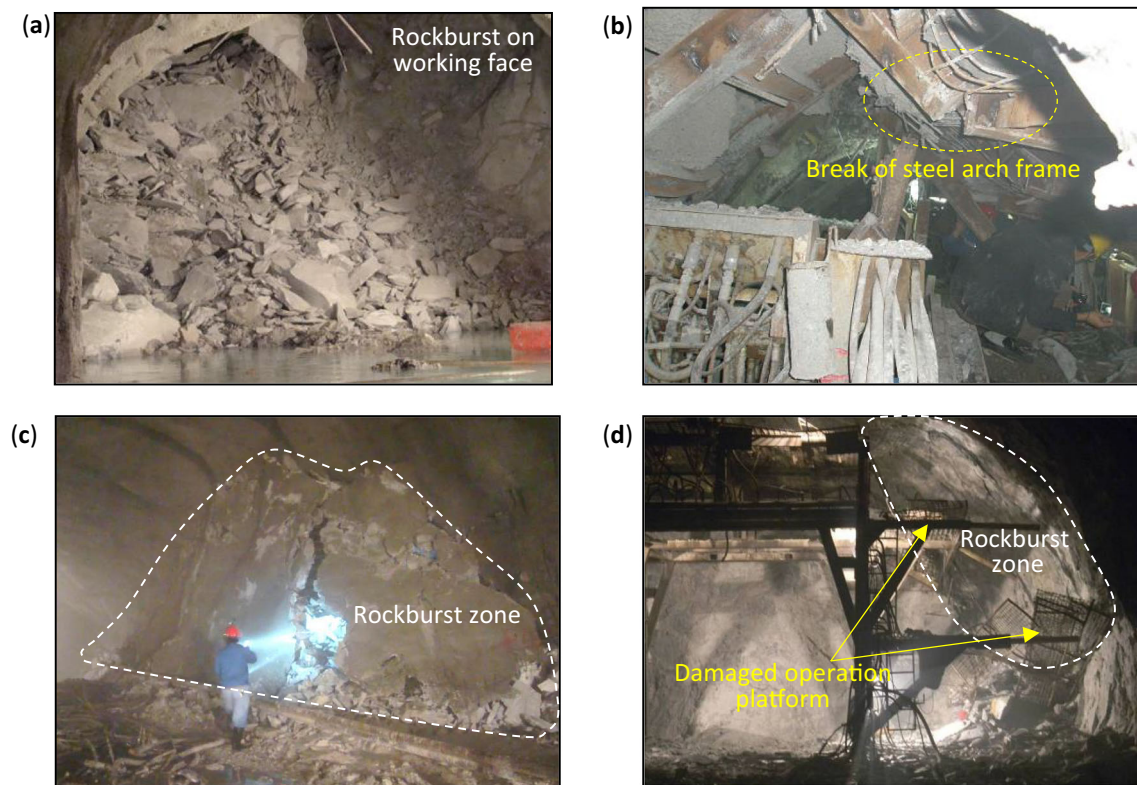


**Fig. 3** Rockbursts that occurred in the Jinping tunnels and the impacts: **a** a violent failure of the rock mass around the working face (Feng et al. 2013), **b** large deformation and breakage of the steel arch frame support

due to a rockburst (Feng et al. 2013), **c** breaking of the rock mass from the tunnel wall with high-strength anchor support, and **d** damage to the operation platform

- Failure depth and approximate volume of the rockburst pit
- Excavation and rock support information
- MS monitoring data
- In situ image

## Method for dynamic estimation of the rockburst scale

### Basic strategy

The occurrence of a rockburst involves a development process that may last from one to several days or even several weeks. Before a rockburst occurs, a series of MS events occur around the zones in which the rockburst will occur. According to the evolution time after excavation, rockbursts are classified by the immediate type and the time-delayed type (Chen et al. 2012; Feng et al. 2013). For the immediate rockburst, these MS events possess temporal, spatial, and energy fractal characteristics that obey objective laws (Feng et al. 2012). Therefore, it is feasible to estimate the immediate rockburst risk by employing these MS data. For the time-delayed rockburst, the studies indicated that the microseismic activity always has a readily observable “sleep” period in the development process (Chen et al. 2012), and early estimation of such a rockburst is difficult. This study focuses on the immediate rockbursts, which are most commonly encountered around the working face in tunneling.

According to the characteristics of immediate rockbursts and the construction process of a drill-and-blast tunnel, the basic strategy for the dynamic estimation of the potential rockburst scale during tunnel excavation is proposed, as illustrated in Fig. 4. So far, the prediction of the exact occurrence time of the rockburst has been a difficult task. The proposed microseismicity-based method provides a strategy for the dynamic estimation of the rockburst development process. When the location of the tunnel working face at time  $t$  is determined, a spatial rockburst estimating volume is obtained. Then, related MS information in the estimating volume before  $t$  should be collected as input to a rockburst estimation model (details will be presented later) to obtain the grade of the rockburst scale. It is recommended that the estimation be conducted every day. However, if the microseismicity is violent, the estimation can be conducted every few hours. The rockburst estimation method is described in detail below.

The microseismicity within the spatial analysis volume differs among zones. For estimating the scale of a potential rockburst, one spatial estimating volume, namely, a limited spatial zone that covers the potential rockburst object and the MS activity which is involved in the rockburst development process, must be selected. However, there was still not much information available regarding the location of the

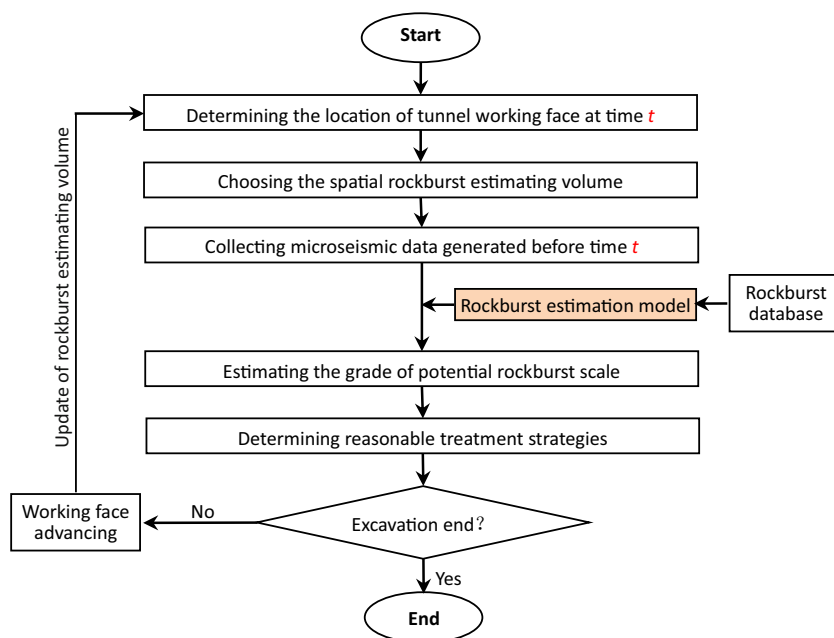
rockburst during the estimation process. Therefore, the size of this estimating volume should be determined based on the spatial distribution of the microseismicity and the unloading zone that is affected by the tunnel excavation. For the Jinping tunnels, the zone from 30 m behind the working face to 10 m ahead (length), from 35 m to the left of the tunnel axis to 35 m to its right (width), and from 50 m above the tunnel axis to 35 m below (height) was selected as the spatial estimating volume via an analysis of the spatial distribution of the rockbursts and associated MS information, along with the engineering characteristics of the tunnels (Feng et al. 2015b), as shown in Fig. 5.

### Grading of the rockburst scale

A rockburst grading scheme of the scale of the failed rock mass is necessary in this study. There are several basic principles that should be considered while establishing a grading scheme of the rockburst scale using  $R_v$ . Firstly, for estimating whether a rockburst will occur or not, “none” should be included in the list of the grading scheme. “None” represents a rockburst scale of zero, namely, no rockburst risk. Secondly, the number of grades should be suitable. Insufficient grades will lead to the loss of guiding effectiveness of estimation results, while too many grades will result in a reduction of the estimation accuracy. It is recommended to divide the rockburst scale into five grades. Thirdly, the volume of a rockburst could vary from very small to very large. The potential range of the rockburst volume that corresponds to a higher rockburst risk is bigger than the volume that corresponds to a lower risk. Therefore, the partitioning of  $R_v$  into increments from small to large is more reasonable.

In addition, for the comparative analysis of the estimation results, it is suggested that the grading of the rockburst scale corresponds to the rockburst intensity classification. That is, the threshold value for each scale grade could be determined based on the volume distribution of rockbursts with different intensities. By March 31, 2011, 206 rockburst cases were collected via in situ investigations, and Fig. 6 shows that the rockburst volume and the associated variation range increase with the rock intensity overall. Herein, the volume value for the quantile that corresponds to 90% of the cumulative frequency was selected as the threshold value of the corresponding grade of rockburst scale. Thus, a preliminary grading of rockburst scale for the Jinping tunnel engineering was constructed, which is presented in Table 1. However, this grading scheme should be determined according to the scope and nature of the project and may differ among engineering projects.

**Fig. 4** Flowchart for dynamic estimation of the potential rockburst scale during tunnel excavation



## Selection and statistical analysis of rockburst samples

### Selection and cluster analysis of samples

Feng et al. (2015b) found that the following MS parameters are suitable for expressing the microseismicity for the estimation or warning of the rockburst risk in the rockburst development process:

- Cumulative number of MS events (expressed as variable  $N$  below)
- Cumulative MS energy (expressed as  $E$ )
- Cumulative MS apparent volume (expressed as  $V$ )
- MS event rate (per day or hour and expressed as  $\dot{N}$ )
- MS energy rate (per day or hour and expressed as  $\dot{E}$ )
- MS apparent volume rate (per day or hour and expressed as  $\dot{V}$ )

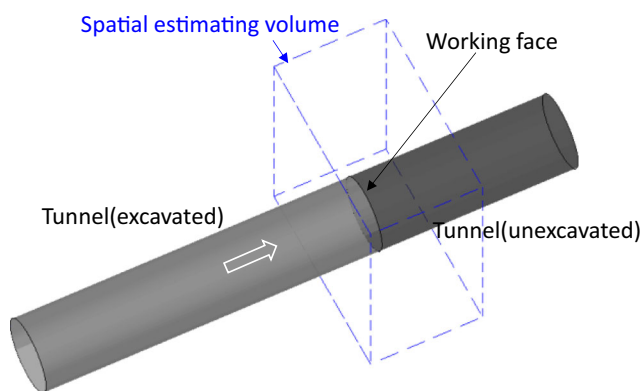


**Fig. 5** Spatial volume used for microseismic estimation of rockburst risk during tunnel excavation

Among these six MS parameters, the cumulative number of MS events represents the number and density of the microfractures that arise inside the rock mass. The cumulative MS energy and cumulative MS apparent volume represent the strength and size, respectively, of the microfractures. Combining the factor of time, these parameters can be used to further interpret the state of the microfractures in the rock mass.

Among the hundreds of rockburst cases that were collected by March 31, 2011, seventy-nine cases that occurred in the zones with MS monitoring and contained all required data were extensively analyzed. The MS data for these cases can be found in the work by Feng et al. (2013). The related microseismic information means the MS activity generated from the spatial estimating volume (Fig. 5) that was determined at the moment before the rockburst occurred. These seventy-nine rockburst cases were divided into five groups according to the scale grade. Figure 7 presents the distribution of the MS information for all cases as a parallel coordinated plot for the graphical presentation of multivariate MS information. The logarithm of the MS parameters including the cumulative energy ( $E$ ), apparent volume ( $V$ ), energy rate ( $\dot{E}$ ), and apparent volume rate ( $\dot{V}$ ) is adopted in this study for convenient processing as it reduces the sizes and volatility of the data. Naturally, data intersection occurred in a few cases that differed in terms of rockburst grade. By and large, however, the value distributions of MS data that corresponded to different grades of rockburst concentrated on different ranges, thereby demonstrating a hierarchical structure from low grade to high grade. Hence, the rockburst scale and the related MS information are strongly correlated, which enabled the development of

**Table 1** Grading of the rockburst scale based on a statistical analysis of hundreds of cases from Jinping tunnels

Grade of the rockburst scale	1	2	3	4	5
Description	None	Small	Medium	Large	Very large
Volume of the rockburst pit/m <sup>3</sup>	0	(0, 3]	(3, 10]	(10, 30]	>30

a quantitative model for rockburst estimation via further sample analysis and data processing.

In order to eliminate the exceptional cases that were inevitably encountered in the data collection process, a filtering selection of typical rockburst samples should be conducted. Cluster analysis, partitioning method for grouping a set of objects (Everitt et al. 2001), can be used to identify the exceptional cases. This method treats the observations in the data as objects that have locations and distances from each other. Therefore, the distances between the rockburst cases in the same scale grade can be calculated and partitioned from close to far by creating a cluster tree. Most of the samples are close to each other and more concentrated. Hence, the cases that are far from the majority could be easily eliminated as exceptional cases. “Distance” in the cluster analysis is defined by the following formula:

$$d(x_K, x_L) = \sqrt{\sum_{j=1}^p (x_{Kj} - x_{Lj})^2} \tag{1}$$

where  $d(x_K, x_L)$  is the Euclidean distance between the  $K$ th and the  $L$ th rockburst cases;  $x_{Kj}$  and  $x_{Lj}$  denote the values of MS parameter  $j$  in the  $K$ th and  $L$ th cases, respectively; and  $p$  is equal to six, namely, the number of MS parameters.

A nondimensional treatment of these MS data should be applied prior to the cluster analysis to remove the distance calculation errors that were generated from the dimensional differences in the MS parameters. The dimensions of various MS parameters can be normalized through a regularization transformation via the following formula (Eq. 2). After the cluster analysis, the remaining seventy-four cases are selected as the typical rockburst samples, and the numbers that correspond to scale grades 1 to 5 are 22, 20, 18, 9, and 5, respectively.

$$X_{ij}^* = \frac{X_{ij} - X_{j,\min}}{X_{j,\max} - X_{j,\min}} \tag{2}$$

where  $i$  is the sequence number of the rockburst samples ( $i = 1, 2, \dots, 74$ );  $j$  is the dimension of the MS data ( $j = 1, 2, \dots, 6$ , which correspond to above six MS parameters);  $X_{ij}$  denotes

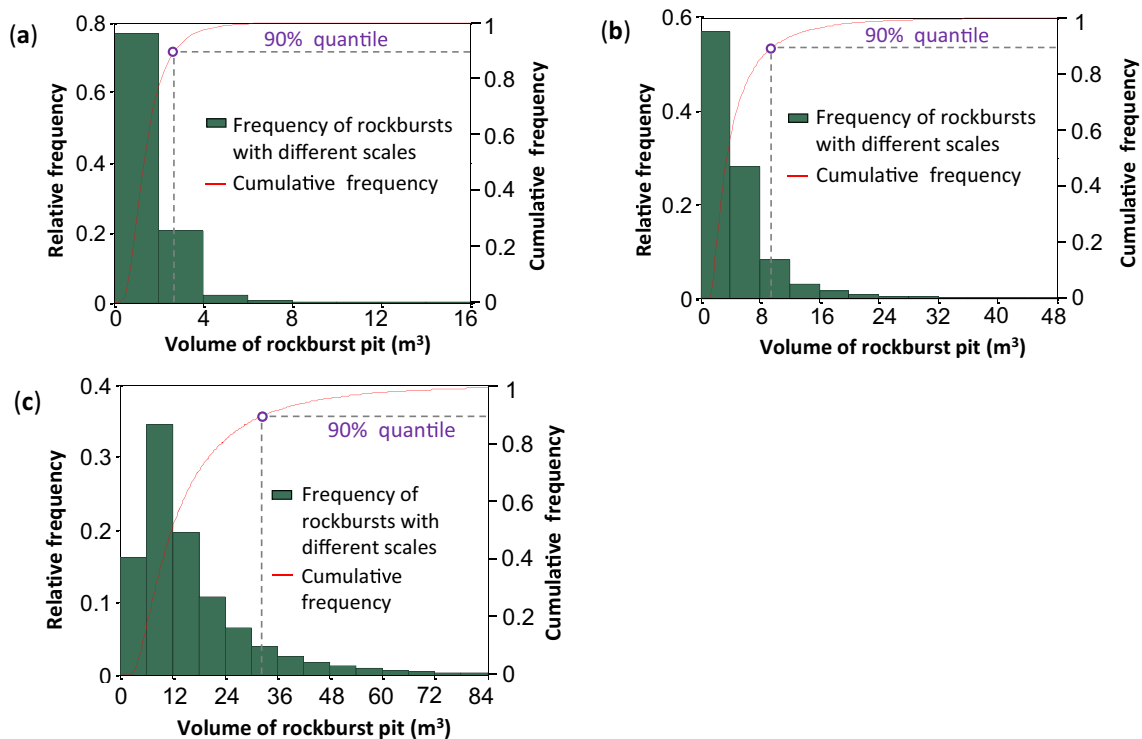


**Fig. 6** Frequency distribution of the volumes of rock mass ejected by rockbursts of various intensities: **a** slight rockbursts (78 cases), **b** moderate rockbursts (89 cases), and **c** intense rockbursts (39 cases)



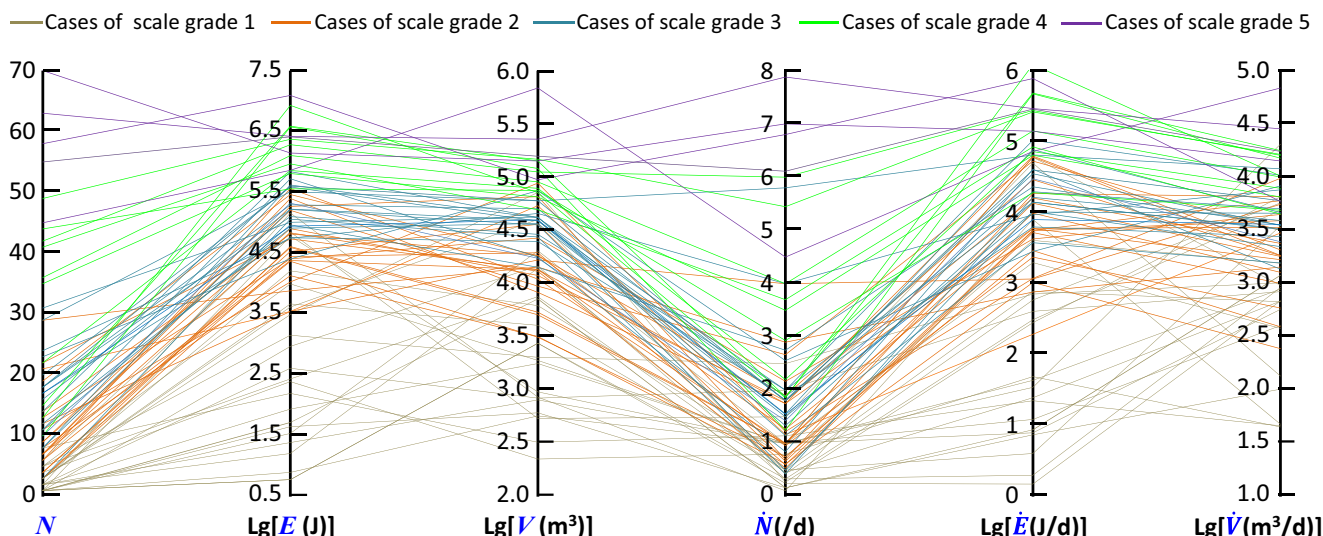


Fig. 7 Parallel coordinate plot for the distribution of six types of microseismic information that correspond to various scales of rockburst cases (The MS data for a rockburst are presented as a corresponding polyline that intersects with six parallel coordinates)

the value of MS parameter  $j$  of sample  $i$  before the normalization;  $X_{ij}^*$  denotes the normalized value of MS parameter  $j$  of case  $i$ ; and  $X_{j,max}$  and  $X_{j,min}$  are the maximum and minimum values of MS parameter  $j$  among all cases. The value range of each MS parameter among all cases is transformed to  $[0, 1]$  via the normalization.

**Statistical regularities of various MS parameters for the rockburst scale**

Based on statistical analysis on these typical samples, the distribution characteristics of each MS parameter ( $N, LgE, LgV, \dot{N}, Lg\dot{E},$  and  $Lg\dot{V}$ ) on various grades of rockbursts could be further illustrated as a statistical box-whisker plot, as shown in Fig. 8. The following regularities of the MS parameters for the rockburst scale are identified:

- (1) As the scale grade of the rockburst increases, the average value of the MS data involved in each parameter increases accordingly, and this is an important indicator for the identification of the rockburst grade. A low-grade rockburst is observed when the values of all the MS parameters were small.
- (2) The distributions and variations of the MS data for the parameters  $\dot{N}, Lg\dot{E},$  and  $Lg\dot{V}$  are similar to those of parameters  $N, LgE,$  and  $LgV,$  respectively. This was further proved by the correlation analysis (Table 2). There are very high correlations between the three pairs of parameters:  $N$  and  $\dot{N}, LgE$  and  $Lg\dot{E},$  and  $LgV$  and  $Lg\dot{V}.$  (The corresponding correlation coefficient for each pair is approximately 0.9.) Thus, the three parameters could almost fully reflect the relationships between the rockburst scale and the microseismicity that are

represented by the six parameters. Since there are a few more mild outliers that are separated from the regular distribution of the MS data for parameters such as  $\dot{N}$  and  $Lg\dot{V},$  the MS parameters including  $N, LgE,$  and  $LgV$  are therefore selected as the final indicators for rockburst scale estimation.

- (3) The interquartile range (the size of the box) and the associated whisker length could reflect the degree of discreteness of the MS data. For one MS parameter, a smaller discreteness of the MS data seems more favorable for the identification of the corresponding rockburst grade. More important to the identification of the rockburst scale are the distribution differences of this MS parameter under various grades. Comparing the overlap ranges in the MS data distribution regarding different grades of rockburst, the sensitivity of each MS parameter to the same rockburst grade differs. For instance, a rockburst of scale grade 1 could be better identified by parameters such as parameter  $N$  or  $LgE,$  while a rockburst of scale grade 5 could be better identified by parameter  $N$  or  $LgV.$  The indicator function of parameter  $LgV$  for a rockburst of scale grade 3 outperforms the parameter  $N$  or  $LgE.$  Therefore, the estimation results should be combined for application to avoid one-sidedness and the limitations of using only a single result.

**Rockburst estimation model**

**Model structure and principles of ANN optimization by GA**

Based on the above rockburst dataset, a series of mathematical tools for processing complex nonlinear problems, such as artificial



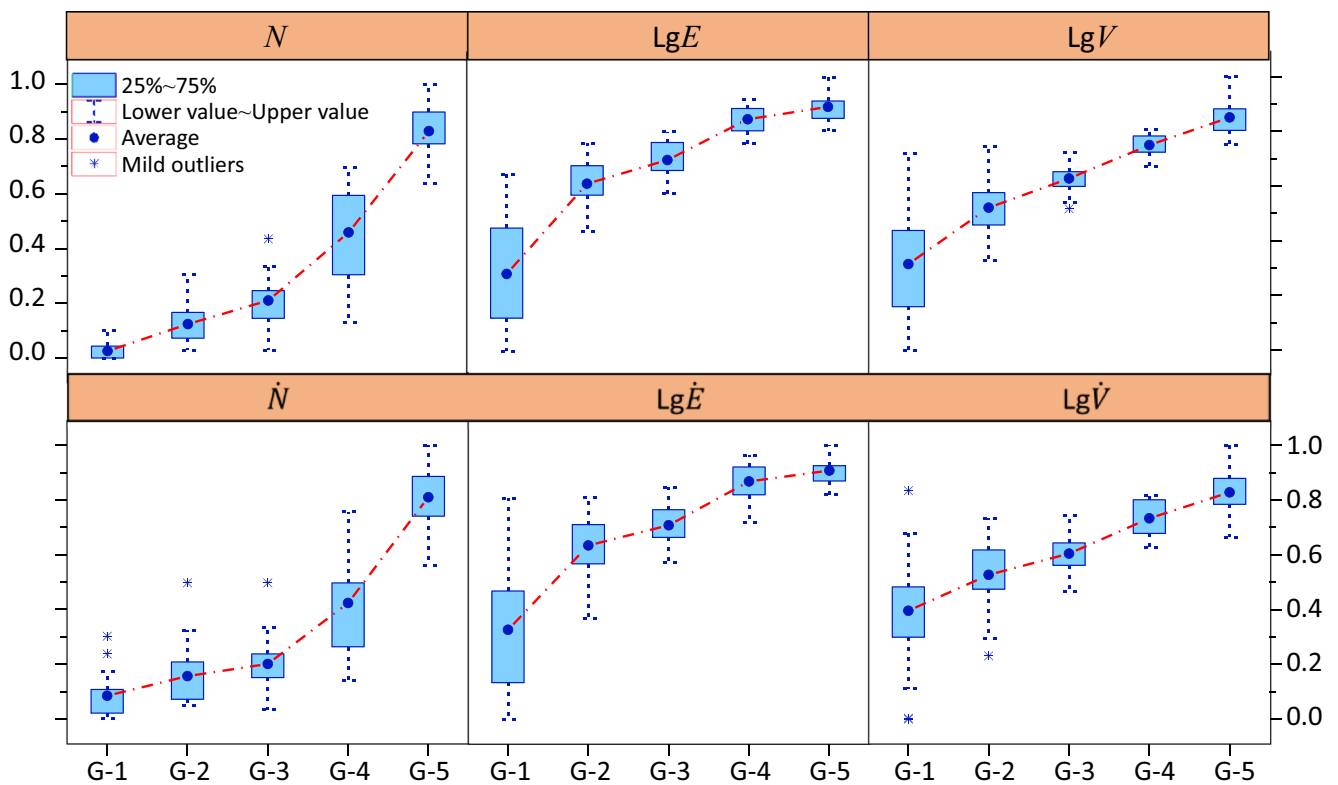


Fig. 8 Box-whisker plot of each MS parameter for five grades of rockburst (G-1 to G-5 denote the rockbursts of grades 1 to 5)

neural networks (Simpson 1990), fuzzy set theory (Dubois and Prade 1980; Adoko et al. 2013), support vector machines (Vapnik 1995), gray systems (Deng 1982), and Bayesian networks (Cooper and Herskovits 1992), can be employed to establish the correlation between the MS parameters and the rockburst scale. In this study, the artificial neural network (ANN) is employed for its nonlinear transformation and highly parallel computing, which is optimized by the genetic algorithm (GA). ANN has been successfully applied as an efficient tool for solving various types of nonlinear prediction problems in underground rock engineering (Suchatvee and Herbert 2006; Abbas and Morteza 2010; Zhou et al. 2015; Chen et al. 2016). The training process of this ANN model for rockburst scale estimation is described as follows.

Table 2 Correlation coefficient matrix between the MS parameters in the sample dataset

	$N$	$LgE$	$LgV$	$\dot{N}$	$Lg\dot{E}$	$Lg\dot{V}$
$N$	1.000	0.601	0.650	<b>0.891</b>	0.552	0.532
$LgE$		1.000	0.672	0.533	<b>0.982</b>	0.529
$LgV$			1.000	0.533	0.614	<b>0.913</b>
$\dot{N}$				1.000	0.552	0.555
$Lg\dot{E}$					1.000	0.542
$Lg\dot{V}$						1.000

Note: The value with bold emphasis means a very high coefficient and indicates that the two corresponding parameters are highly correlated.

A neural network is a network of simple processing elements (artificial neurons) that can display complex global behavior as determined by connections between the processing elements and their parameters (Simpson 1990). In machine learning, ANN is a family of statistical learning models that are inspired by biological neural networks and is used to estimate functions based on many inputs that are typically unknown. According to the analyses above, an ANN estimation model that accepts the three MS parameters, namely,  $N$ ,  $LgE$ , and  $LgV$ , as inputs and the grade of the rockburst scale as output is established, the structure of which consists of four layers in total, namely, an input layer, two medium hidden layers, and an output layer, as illustrated in Fig. 9a. The model can be trained by above sample dataset and further optimized via the GA to obtain the best structures and initial weights of the network.

As the basic element in the ANN, the common principle of the operational model for a single neuron is illustrated in Fig. 9b. The training process of an ANN model typically begins randomly. In order to reduce the differences between the calculated and expected outputs, a back-propagation algorithm is used to update the weight values in the ANN training process. The back-propagation neural network (BPNN) is a multilayer feed-forward algorithm that is trained via backward error propagation (Fig. 9c). Furthermore, to overcome the inconsistent and unpredictable performance from trapping in a local minimum in the conventional back-propagation neural

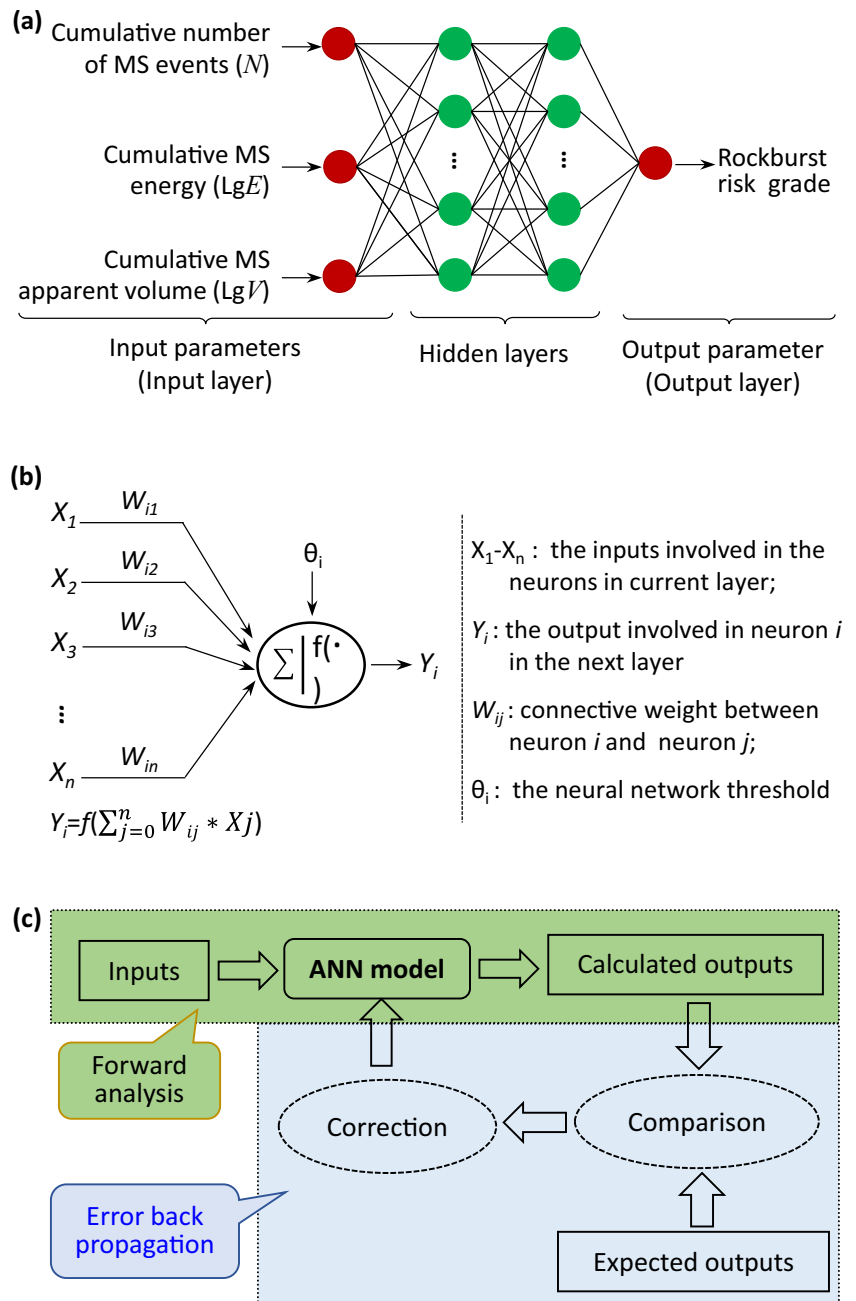
network, a GA-improved training algorithm (Goldberg 1989) has been proposed for optimizing the parameter settings, especially the number of neurons in each hidden layer during the training process. By employing the GA, the structure parameters of hidden layers can be evolved in the outer GA procedures. Then, the initial weights of the model structure are evolved in the inner GA procedures, where a back-propagation algorithm is used to evaluate the fitness of the initial weights. *Fitness* is an important indicator which is optimized via natural selection in a GA. For controlling the evolution process, the fitness of

each generated initial weight set is calculated according to the difference between the calculated results and the expected results, which can be expressed by the following Equation if the mean square error is used.

$$fitness = \frac{1}{n} \sum_{i=1}^n (u_i - u_i^*)^2 \tag{3}$$

where  $u_i$  and  $u_i^*$  are the calculated result and the expected result, respectively, and  $n$  is the number of learning samples.

**Fig. 9** Basic strategy of the ANN model for rockburst estimation: **a** the structure of the four-layer ANN model, **b** the operational model of a single neuron (the basic element in the ANN), and **c** the fundamentals of the back-propagation neural network



### Training samples and parameter settings

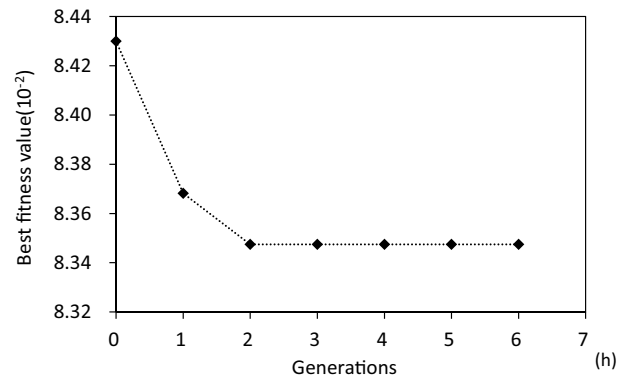
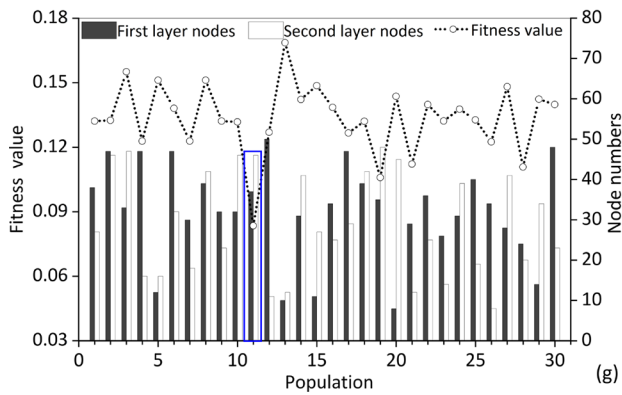
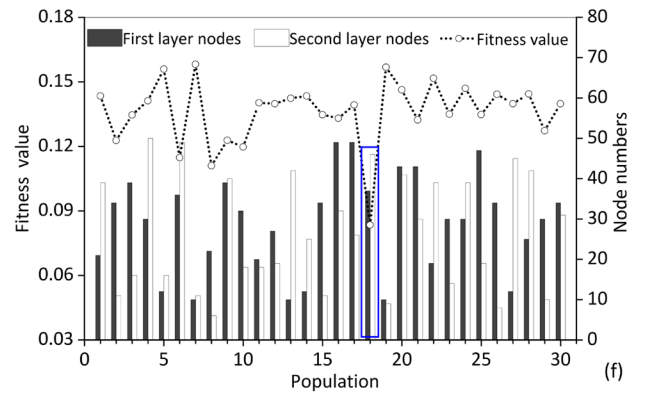
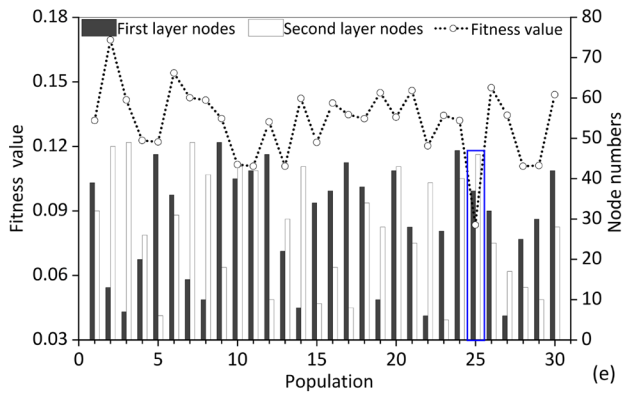
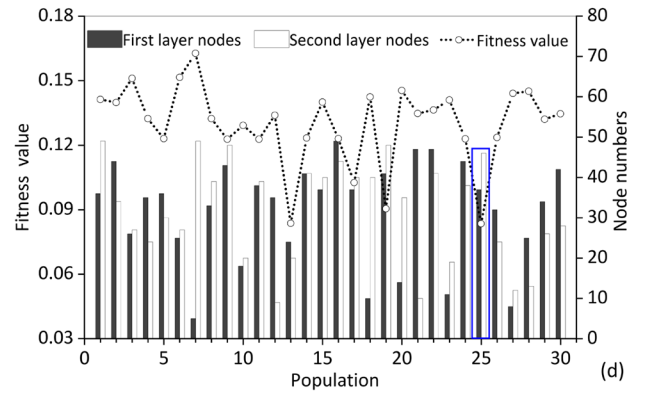
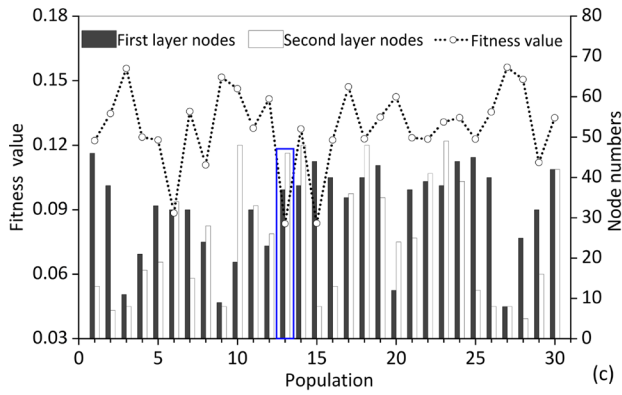
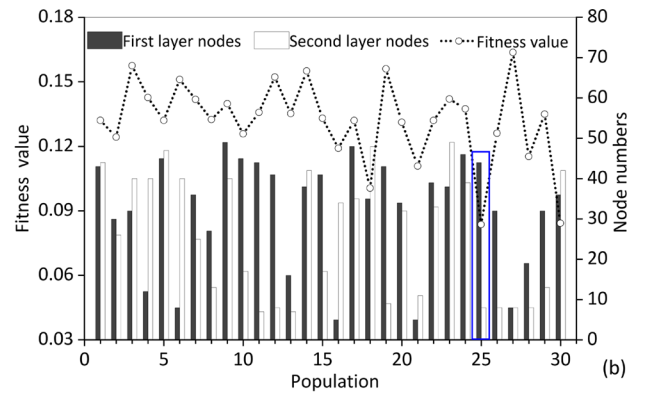
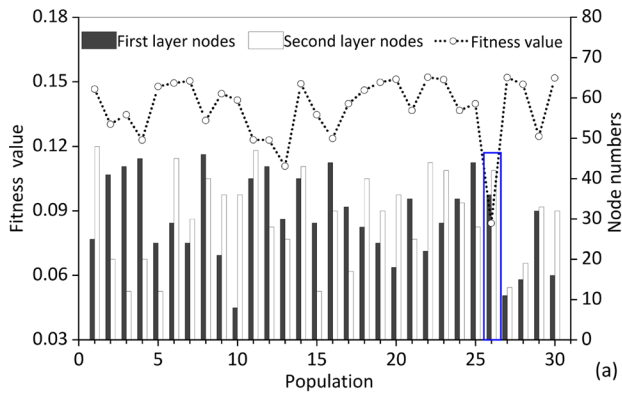
ANN is a data-based method, and the seventy-four cases used for ANN training were randomly split into two parts: learning samples and testing samples. The training data should be representative and evenly spread over the solution space, and the ratio of learning samples and testing samples was determined from the relevant literatures (Zhou et al. 2012; Sen et al. 2012; Sezer et al. 2014; Chen et al. 2016). In this study, 80% of the available data (fifty-nine cases) were regarded as the learning dataset for ANN training of the estimation model, and the reserved fifteen cases are used as the testing dataset for the performance evaluation of the ANN-based model. Some cases used are listed in Table 3 as examples. The data types of the three input parameters are set as  $N$ ,  $LgE$ , and  $LgV$ , respectively. However, the input data typically must be normalized to avoid unnecessary numerical problems that are caused by dimensional differences and to accelerate the convergence of the neural networks, as expressed in Eq. 2. The output data are set

as follows, [1, 0, 0, 0, 0], [0, 1, 0, 0, 0], [0, 0, 1, 0, 0], [0, 0, 0, 1, 0], and [0, 0, 0, 0, 1], which denote the rockbursts of scale grade 1, grade 2, grade 3, grade 4, and grade 5, respectively.

A series of parameters must be set in the GA and ANN procedures. In the outer GA procedure, the hidden layers constitute a feed-forward structure for a general function approximation, and a search space that ranges from 5 to 50 is set for the determination of the number of hidden layer nodes. The population size is set to 30, and the crossover probability and mutation probability are set to 0.7 and 0.1, respectively. In the inner GA procedure, the number of initial weights changed according to the values of the structural parameters. The range setting of the initial weights in the GA optimization procedures can substantially influence the convergence speed and training accuracy. According to studies from Chen et al. (2016), a smaller range of initial weights could lead to faster convergence and higher training accuracy through the analysis and comparison of several groups of recommended weight ranges, which include [-0.5, 0.5] (Sietsma and Dow 1999),

**Table 3** Learning and testing samples for ANN training of the rockburst estimation model

Sample types	No.	Input: MS monitoring information			Output: rockburst grade				
		$N$	$LgE$ (J)	$LgV$ (m <sup>3</sup> )	1	2	3	4	5
Learning samples	1	1	2.970	4.164	1	0	0	0	0
	2	5	3.996	3.279	1	0	0	0	0
	3	3	3.616	4.603	1	0	0	0	0
	20	8	2.197	2.511	1	0	0	0	0
	21	3	3.668	3.609	1	0	0	0	0
	22	7	5.269	4.817	0	1	0	0	0
	23	9	5.204	3.977	0	1	0	0	0
	41	21	3.543	4.732	0	1	0	0	0
	42	14	4.818	4.266	0	1	0	0	0
	44	23	4.408	4.873	0	0	1	0	0
	45	14	5.841	4.622	0	0	1	0	0
	59	31	5.008	4.627	0	0	1	0	0
	60	17	4.944	4.598	0	0	1	0	0
	61	22	5.859	4.895	0	0	0	1	0
	62	49	6.373	5.168	0	0	0	1	0
Testing samples	68	42	6.284	5.050	0	0	0	1	0
	69	10	6.576	5.081	0	0	0	1	0
	73	58	7.094	4.975	0	0	0	0	1
	74	63	6.420	5.357	0	0	0	0	1
	5	6	4.850	2.735	1	0	0	0	0
	17	4	2.390	2.354	1	0	0	0	0
	26	7	4.381	4.132	0	1	0	0	0
	35	12	3.543	4.223	0	1	0	0	0
	49	20	5.589	4.589	0	0	1	0	0
	55	11	5.724	4.251	0	0	1	0	0
62	36	6.105	4.956	0	0	0	1	0	
72	70	6.147	5.152	0	0	0	0	1	





◀ **Fig. 10** Optimization results of hidden layer nodes and the best fitness value over six generations: **a** the initial generation, **b** the first generation, **c** the second generation, **d** the third generation, **e** the fourth generation, **f** the fifth generation, **g** the sixth generation, and **h** the evolution of the best fitness value

$[-0.25, 0.25]$  (Gallagher and Downs 2003; Kavzoglu and Mather 2000), and  $[-0.1, 0.1]$  (Rayburn and Klimasauskas 1990). Therefore, the initial weight range in this work is set as  $-0.1$  to  $0.1$ . In addition, binary coding is adopted and fitness-proportionate selection is used as the selection strategy in GA procedures. The fitness function is a standard cost function. The genetic operators employ uniform hybridization and uniform mutation.

The learning rate and momentum coefficient are critical for network convergence and stability. The lower learning rate will lead to longer learning time, while a lower learning rate is more conducive to network convergence. Thus,  $0.1$  is selected as a relatively small value in the training. The momentum coefficient is typically added as a parameter to avoid the local minimum point in the training process, and it is set to  $0.6$  herein. The learning and testing termination errors are set to  $1 \times 10^{-5}$  and  $1 \times 10^{-8}$ , respectively. More attention should be paid to whether an overfitting phenomenon occurs under very small learning and testing errors and a very large number of allowed iterations.

### Training results

Figure 10 presents the optimization results of hidden layer nodes and the fitnesses of individuals that are involved in the ANN structure over six generations, based on a GA-based global search that uses a series of genetic operations including reproduction, crossover, and mutation. The optimization was successfully completed with stable convergence when the GA procedure ran to the second generation (see Fig. 10h), in which the best fitness value was  $0.0835$  and the

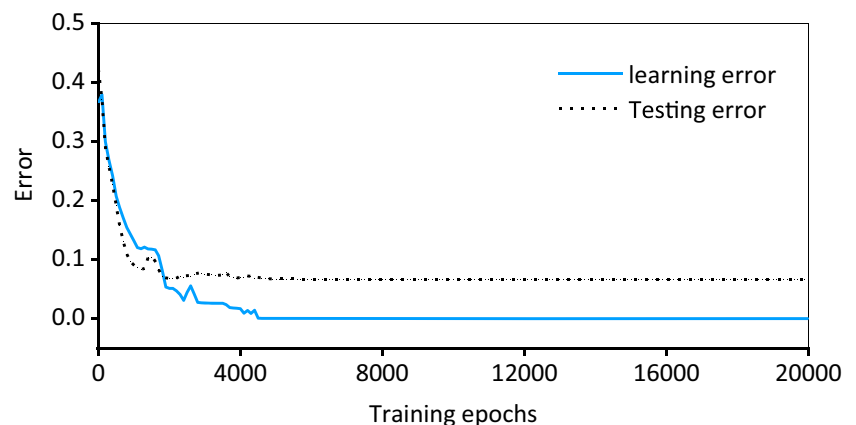
corresponding optimal numbers of nodes in the two hidden layers were  $37$  and  $46$ .

According to the optimized parameters, a final training process was conducted to establish an estimation model of the rockburst scale. As shown in Fig. 11, the training process finished successfully when the testing and learning errors were minimized without overfitting. Figure 12 compares the results that were calculated by using the trained ANN model with the expected results for all samples. The rates of correct rockburst estimation of the learning samples and testing samples are  $100$  and  $93.33\%$ , respectively. Hence, this rockburst estimation model has satisfactory application prospects for known samples and for unknown samples that are not included in the learning process.

### *k*-fold cross validation

The *k*-fold cross validation (Delen et al. 2005; Sen et al. 2012), also called rotation estimation, can be employed as an effective approach to minimize the bias associated with the random sampling of the training. In *k*-fold cross validation, the complete dataset (*D*) is split randomly into *k* mutually exclusive subsets (the folds:  $D_1, D_2, \dots, D_k$ ) with approximately equal size. The classification model is then trained and tested *k* times. Each time, it is trained on all but one folds ( $D_i$ ) and tested on the remaining single fold ( $D_i$ ). Finally, these *k* individual accuracy results from the *k*-fold cross validation can be averaged to produce a single result as the overall accuracy. In this study, 5-fold cross validation was used; namely, the complete seventy-four samples were divided randomly into 5 exclusive subsets. The sizes of samples in the five subsets were  $15, 15, 15, 14,$  and  $15$ , respectively. The class distribution in the five subsets was nearly the same as the original dataset. In particular, the testing dataset used in the above modeling was treated as one of the five subsets (Train-3 in Table 4). The training like the process as illustrated above was performed for five times in total, and the cross validation result is shown in Table 4. It indicated that the accuracies of the models trained

**Fig. 11** Error variation of the neural network classifier for learning and testing samples during training process



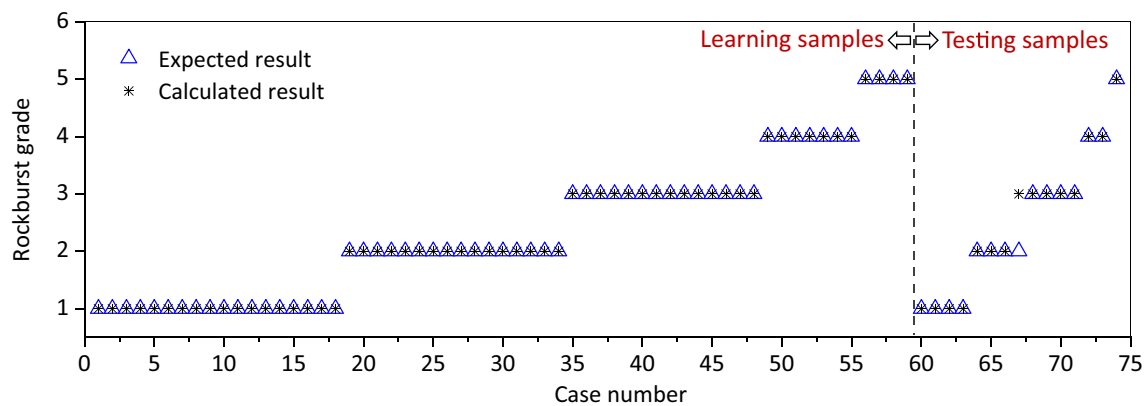


**Fig. 12** Comparison of the calculated and expected results of the learning and testing cases with the trained ANN model

by five times, based on different datasets assigned from random sampling, were different and fluctuated in a certain range. Nevertheless, the testing accuracy of the trained model was at least more than 85.71 % and reached 90.48 % in terms of the average value under random sampling. The results showed that the model trained by these rockburst samples could work for most cases.

### Dynamic updating

Dynamic updating is essential for ensuring the performance of the estimation method in optimization, and it can be implemented by the following two mechanisms in this method.

As discussed previously, the exact rockburst occurrence time remains unpredictable. The occurrence of a rockburst often involves a development process that may last from one to several days; hence, a dynamic estimation process is always required. The estimated result at time  $t$  indicates that there may be a rockburst risk nearby at a later time, but rockbursts do not always occur instantaneously. Regardless of whether this estimated result is verified later or not, the rockburst estimated results should be updated timely when either new monitoring microseismic information arises in the current rockburst estimating volume or the working face advances. Thus, a series of updates of the estimate may need to be conducted before a rockburst occurs, especially for a rockburst that has a long development process. The estimation process will be

successful if the latest estimation result before the occurrence of a rockburst matches the actual rockburst scale. A case that involves the dynamic estimation process will be presented later to demonstrate the estimation updating process more clearly.

Once the proposed method has been applied to estimate the rockburst risk, a new case will emerge. This case should be added into the rockburst database (as a successful or unsuccessful case). As the rockburst estimation process continues with the tunnel excavation, the ANN estimation model will be improved and optimized continuously as the rockburst database updates.

## Engineering validation

### A case study for dynamic rockburst estimation

As an example, a typical rockburst case that involves the dynamic estimation process is firstly presented. On August 9, 2011, the upper benching face of the #3 headrace tunnel was at chainage K8+728 moving eastward, where the burial depth was close to 2500 m. The surrounding rock was marble and characterized by its brittleness and low TS/UCS. There were some rigid joints without fillings in local positions of the wall, as shown in Fig. 13. The fresh surrounding rock had good quality and was ranked as “III,” according to Chinese

**Table 4** The performance of five-fold cross validation for the ANN training of rockburst estimation

	Learning dataset	Testing dataset	Testing accuracy	Total mean squared error	Squared correlation coefficient
Train-1	Subsets 2–5	Subset 1	86.67%	1.21E-2	0.925
Train-2	Subsets 1 and 3–5	Subset 2	100%	1.06E-5	0.999
Train-3	Subsets 1–2 and 4–5	Subset 3	93.33%	5.41E-3	0.966
Train-4	Subsets 1–3 and 5	Subset 4	85.71%	1.03E-2	0.936
Train-5	Subsets 1–4	Subset 5	86.67%	1.09E-2	0.932
Average			90.48%	7.74E-3	0.952

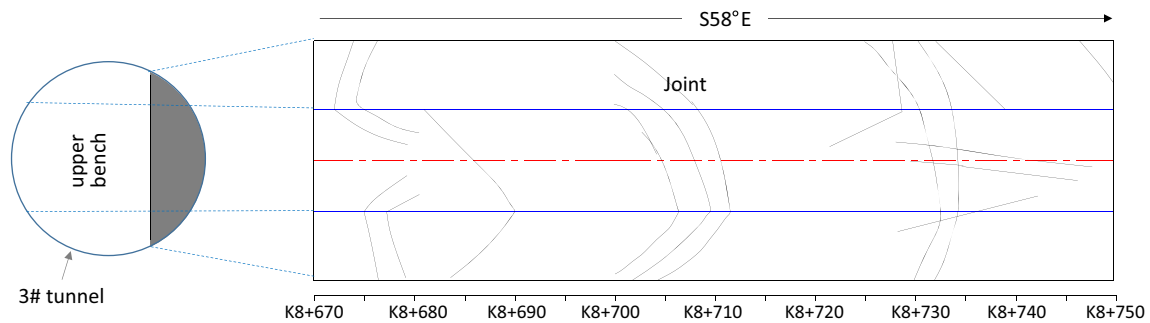


Fig. 13 The planar distribution of geological information of the tunnel wall

“Standard for engineering classification of rock mass,” and therefore might be subjected to the rockburst hazards.

To estimate the subsequent rockburst risk in that scene, the rockburst estimating volume was firstly determined, the range of which along the tunnel axis was the zone from K8+698 to K8+738, namely, the zone from 30 m behind the working face to 10 m ahead. The spatial distribution and temporal evolution of the microseismic events that developed in the spatial estimating volume by 24:00 Aug. 9 are presented in Fig. 14a, b, and Table 5 summarizes the detailed information of the precursory microseismicity. Then, these MS data were input into the ANN estimation model that was trained by the cases that were previously collected, and the output result was [0, 0, 0, 1, 0]; namely, a rockburst with the scale of grade 4 (10~30 m<sup>3</sup> in volume) would occur in the current spatial estimating volume on August 10, 2011, or later.

Recent development in numerical methods delivers strong supports for the behavioral study of underground constructions under a set of predefined initial environments like boundary conditions, in situ stresses, and geometry (Das et al. 2017). In order to further estimate the potential rockburst area on the cross section of the tunnel, the elastic analysis of stress concentration induced by the excavation was performed through numerical simulation. The FLAC<sup>3D</sup> program (Itasca, 2012) which has been commonly used in geotechnical engineering field was chosen herein to achieve it. According to mechanical tests and back analysis, the elastic modulus and Poisson’s ratio of the rock mass were determined as 19 GPa and 0.23, respectively. As shown in Fig. 15, the simulation result indicated that the maximum stress concentration area induced by the upper benching would occur in the north sidewall, and the stress redistribution in the south sidewall also needed attention. Actually, the stress concentration in the two

opposite sidewalls with high rockburst risk was relevant to the in situ stress orientation.

At 9:10 a.m. on Aug. 10, 2011, an intensive rockburst occurred in the south sidewall of the tunnel from chainage K8+700 to K8+728, which made a loud noise on site. The position of the rockburst on the tunnel cross section matched the simulation result, and the maximum depth of this rockburst pit was 1.2 m, as presented in Fig. 14c. According to an in situ investigations, the volume of the rockburst pit was approximately 20~25 m<sup>3</sup> and graded as 4, which agreed with the estimated result obtained by the ANN model. As the rockburst undergoes its development process, which may last several days, the estimations must be conducted dynamically. Figure 16 presents the dynamic estimation process of this case with the tunnel excavation, in which the microseismicity in the related spatial estimating volume and the associated estimation result, along with actual scenario, were provided. The results demonstrate that new rockburst estimating volume was constantly determined with the advance of the working face (Fig. 16a), and the microseismicity-based estimation result was updated accordingly (Fig. 16b). The rockburst risk around the working face increased from grade 2 to grade 3 since August 4 and remained at grade 3 until Aug. 7. Then, the excavation stopped, and the working face remained at chainage K8+728, while the microseismicity in the spatial estimating volume was still active. According to the estimation at 24:00 on Aug. 9, the rockburst risk near the working face in the subsequent days (Aug. 10 or later) increased to grade 4. A rockburst of scale grade 4 occurred approximately 9 h later, and the occurrence and the scale of this rockburst were well estimated by the precursory microseismicity in the rockburst estimating volume and an ANN estimation model.

In this case, the estimation could also be conducted every few hours during the days in which the rockburst risk began increasing from grade 3 to grade 4. Therefore, it is necessary to ascertain whether the estimated result of rockburst scale changes during the last 9 h before the rockburst occurred. The distribution of all MS events that occurred before 9:10 a.m. on Aug. 10 in the rockburst estimating volume is presented in Fig. 17. Compared with the precursory microseismicity that was collected by 24:00 on Aug. 9, three new MS events

Table 5 Microseismicity in the rockburst estimating volume by 24:00 August 9, 2011

	Microseismic parameters		
	<i>N</i>	<i>E</i> (J)	<i>V</i> (m <sup>3</sup> )
Value	45	6.353×10 <sup>4</sup>	6.886×10 <sup>4</sup>

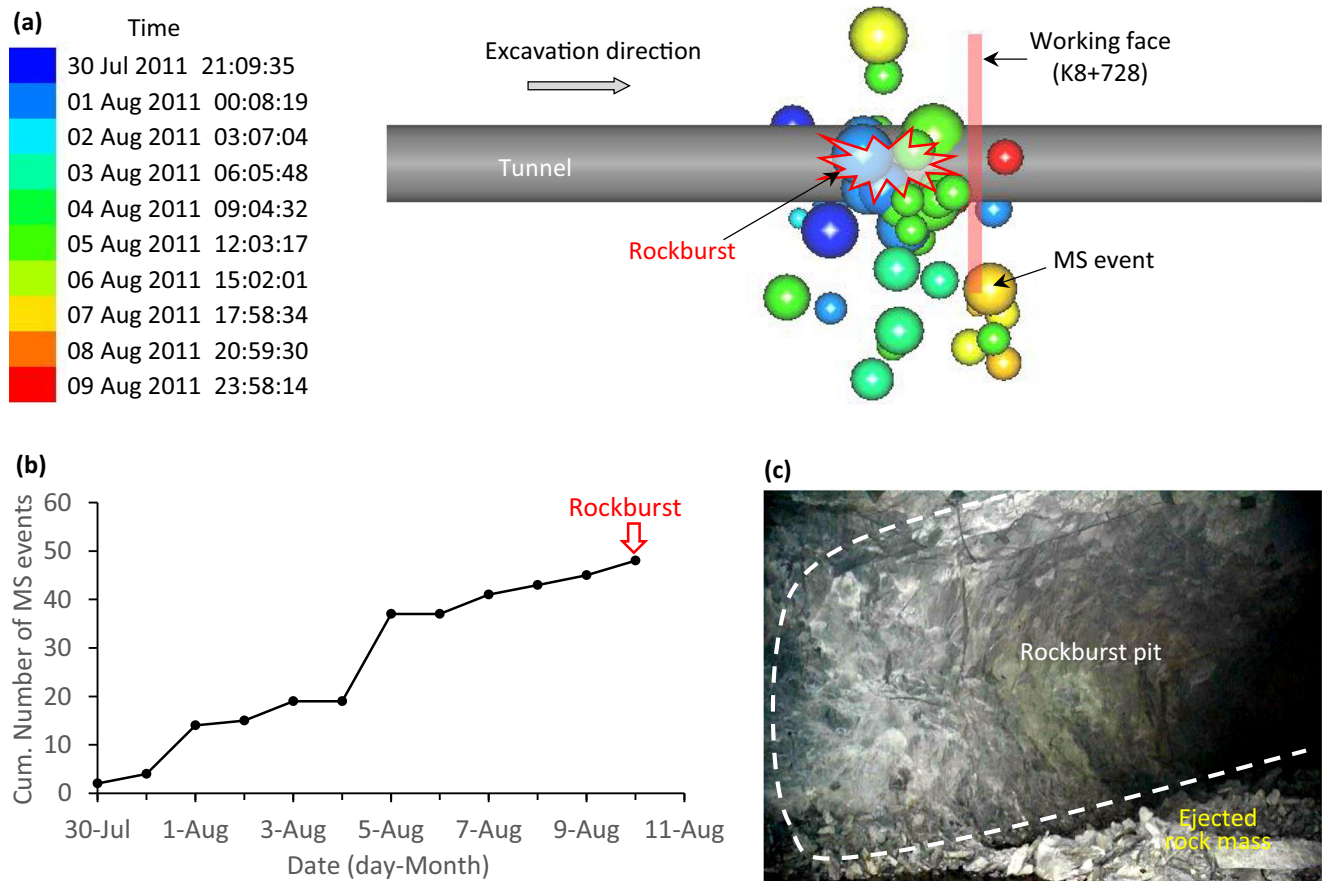


**Fig. 14** Results of MS monitoring on the zone from K8+698 to K8+738 of #3 headrace tunnel: **a** the spatial distribution of MS activity in the rockburst estimation volume (sphere color represents the time of the

MS event and the size of the sphere represents the energy of event), **b** curve of the cumulative number of MS event vs time, and **c** photograph of the rockburst at chainage from K8+700 to K8+728

occurred in the last 9 h, and the values of corresponding MS parameters  $N$ ,  $E$ , and  $V$  increased to 48,  $6.395 \times 10^4$  (J), and  $6.988 \times 10^4$  (m<sup>3</sup>), respectively. The new calculation demonstrated that the estimated rockburst scale still remained grade 4 and matched the actual rockburst scenario. In this case, the dynamic estimation process is presented as a series of estimations that were conducted daily as an example. If the rockburst estimating volume continues to produce microseismic events

and the rockburst risk is at a high grade, the estimation result should be updated every few hours instead of once a day to timely track and manage the rockburst risk.

**Validation results of multiple cases**

To further validate the applicability of the proposed estimation method of the rockburst, thirty-one cases that

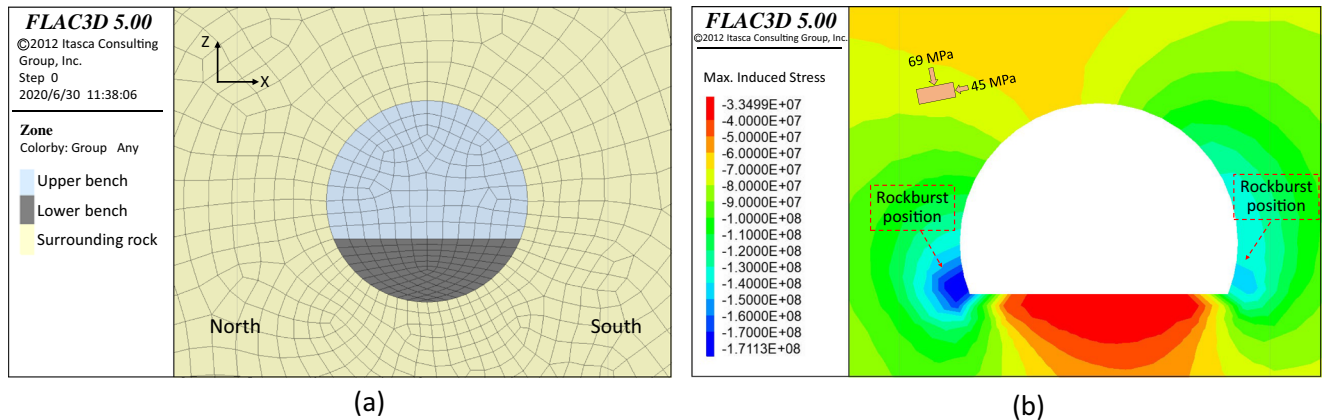


**Fig. 15** Stress analysis for estimating the rockburst position: **a** the grid model and **b** simulation result of maximum induced stress



occurred in parts of the #3 and #4 Jinping tunnels, which had a cumulative length of 1.85 km (3#K5 + 750 ~ K6 + 200, 3#K8 + 600 ~ K9 + 000, 4#K7 + 750 ~ K8 + 350, 4#K8 + 600 ~ K9 + 000) and were excavated after March 31, 2011, under continuous MS monitoring, have been extensively analyzed and studied. Figure 18a presents the geological cross section along the related tunnels and the distribution of these rockburst cases at various scales. The agreement between the rockburst estimation results and the actual situations is presented in Fig. 18b, which shows that approximately 83.9% of the rockburst cases were estimated reliably. Hence, the proposed estimation method is highly applicable in most cases. There are five cases in which the estimated results were inconsistent with the actual scenarios, indicating that this method still have some limitations for a few cases, and these cases can be divided into two types. (1) For case 6, 16, or 25, in which the estimated scale was one grade higher or lower than the actual scale, there was a substantial dispersion of the MS parameter values. The microseismicity of these rockburst cases differed from the statistical characteristics of rockbursts of that grade but was more similar to the characteristics of rockbursts with an adjacent grade, which hindered the exact identification. (2) In the monitoring process, for only a few rockbursts (less than 10%), the associated precursory microseismicities were not readily observed (Feng et al. 2015b; Liu et al. 2016). This causes the estimated scale of a rockburst to be far lower than actual value, such as in cases 22 and 29, as shown in Fig. 18b, in which each had a low estimated grade (1 or 2) but a relatively high actual grade (3 to 4). In the modeling process, these individual cases were often treated as exceptional cases (as stated above) and easily to be removed by the cluster analysis. For the rockbursts that lack readily observable MS precursors, additional investigation is needed to improve the interpretation of the rockburst mechanism.

It is noted that the rockburst estimation model was constantly updated and improved as new cases occurred during the engineering validation process. At last, the rockburst estimation model was updated by 110 cases (sum of 79 and 31) in total by repeating previous training process which mainly includes the cluster analysis, ANN training, and  $k$ -fold cross validation. The new five-fold cross validation regarding the trainings by more samples showed that the updated model had the average accuracy of 91.30%, which was a bit higher than that (90.48 %) of the old model concerning seventy-four cases. Moreover, the differences in the testing accuracies of the five trainings were further reduced (within 5%); that is to say, the accuracy fluctuation of the model trained under random sampling is decreased as the size of the dataset used for training increases.

## Discussion

### Rockburst prediction from both intensity and scale

The rockburst intensity is a common indicator for the evaluation of the failure degree of a rockburst. The rockburst warning formula, proposed by Feng et al. (2015b), can be used to calculate the probabilities of rockburst risk with various intensities during the rockburst development process, which is expressed as follows:

$$P_i = \sum_{j=1}^n w_j \cdot P_{ji} \quad (4)$$

where  $i$  is the rockburst intensity (extremely intense, intense, moderate, slight, or none);  $j$  denotes the microseismic parameter ( $N$ ,  $E$ ,  $V$ ,  $\dot{N}$ ,  $\dot{E}$ , and  $\dot{V}$ );  $n$  is the number of MS parameters that are used to express the microseismicity;  $w_j$  is the weighting coefficient;  $P_{ji}$  is the functional relationship between microseismic parameter  $j$  and rockburst intensity  $i$ ; and  $P_i$  is the probability of rockburst intensity  $i$ .

As stated in the "Introduction" section, the failure scale of surrounding rock caused by a rockburst is typically proportional to the rockburst intensity in most cases, but not all. The estimation method proposed in this study could be used separately to focus on the dynamic estimation of the potential rockburst scale or used as a complementary approach to add details on the characteristics of the unknown rockburst risk besides the intensity prediction. Studies on two cases are presented to demonstrate the advantages of using a combination of the rockburst estimates from the two perspectives.

Taking the case analyzed in the above section as the first example, the rockburst warning formula (Eq. 4) was used to assess the rockburst risk based on the same microseismicity data that were collected up to Aug. 9. The warning results are as follows:  $P_{\text{none}}=0.0\%$ ,  $P_{\text{slight}}=11.2\%$ ,  $P_{\text{moderate}}=29.8\%$ , and  $P_{\text{intensive}}=59.0\%$ . The estimation result that was calculated via the ANN model that is presented in this study was grade 4. Hence, there was a high risk of an intensive rockburst of grade 4 in scale in the rockburst estimating volume (3#K8+698 ~ K8+738) on Aug. 10, 2011, or later. The actual scenarios described above prove the correctness of both assessment results.

At 7:10 p.m. on November 21, 2011, another rockburst occurred in the north sidewall of the tunnel from chainage 3#K8+950 to chainage 3#K8+990 when the working face advanced to chainage 3#9+000. The position of this rockburst on the tunnel cross section is consistent with the stress analysis result which is almost similar to Fig. 15. Figure 19a presents the spatial distribution and evolution of the MS events that developed in the rockburst estimating volume up to Nov. 10, and Table 6 summarizes in detail the information on the precursory microseismicity. According to Eq. 4, the warning

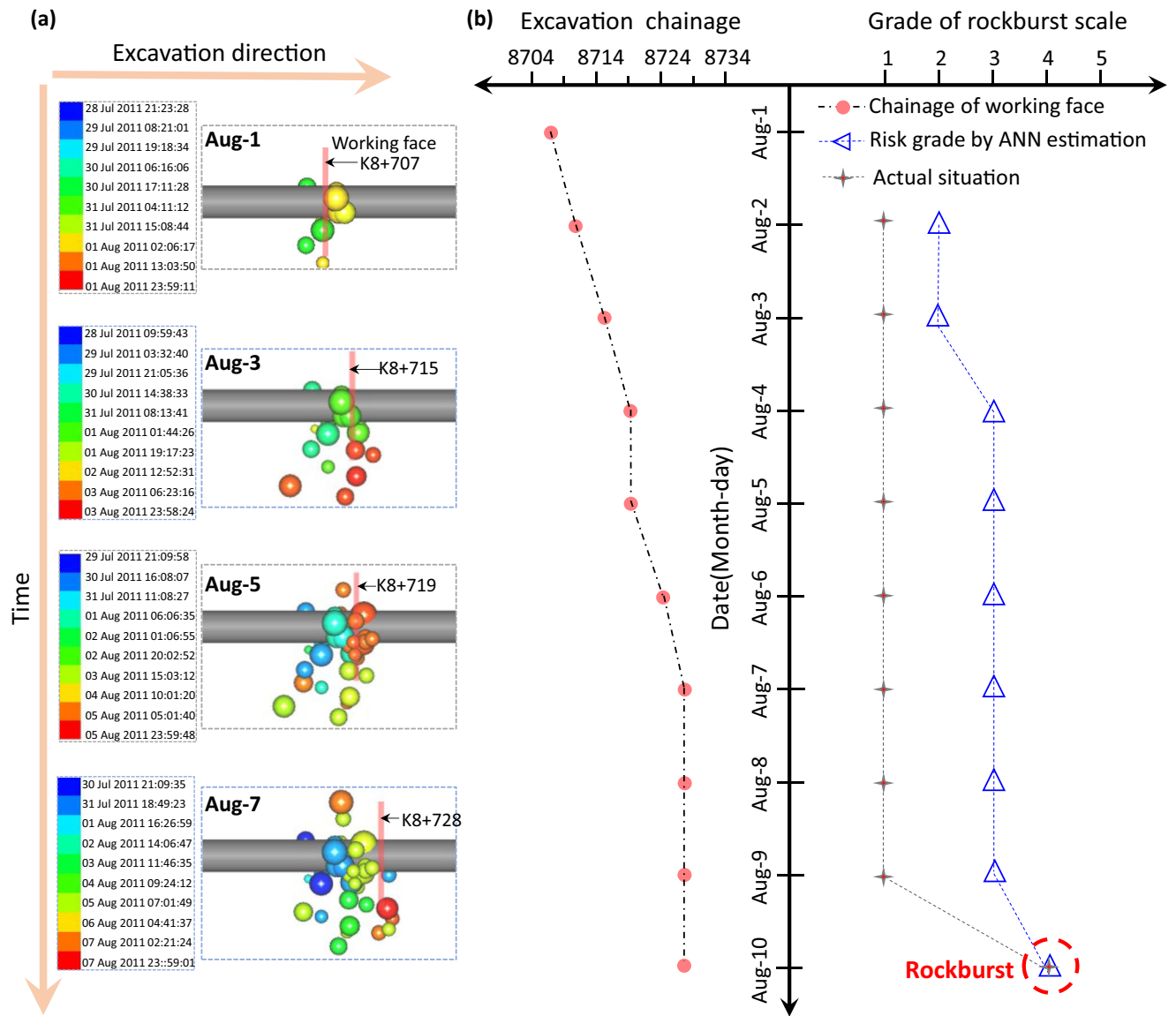


**Fig. 16** Dynamic estimation process of the rockburst risk during the period from Aug. 1 to Aug. 10: **a** evolution of the MS activity in the associated spatial estimating volume with the advance of the working face

and **b** evolution of the corresponding estimation result or rockburst risk (the risk grade of the day ( $t$ ) was estimated by MS data that were collected the day before ( $t-1$ ))

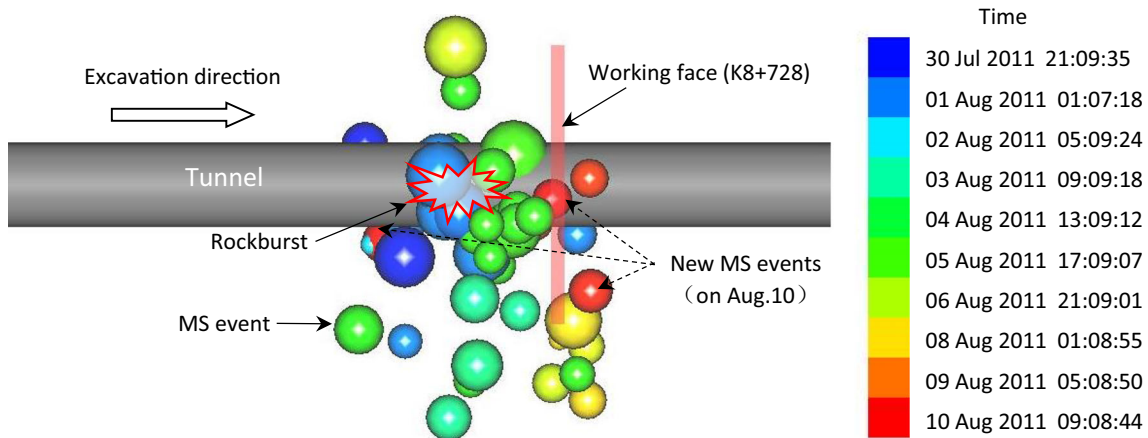


**Fig. 17** Spatial distribution of the MS activity in the rockburst estimating volume before 9:10 a.m. on August 10, 2011 (a larger sphere corresponds to more released energy)

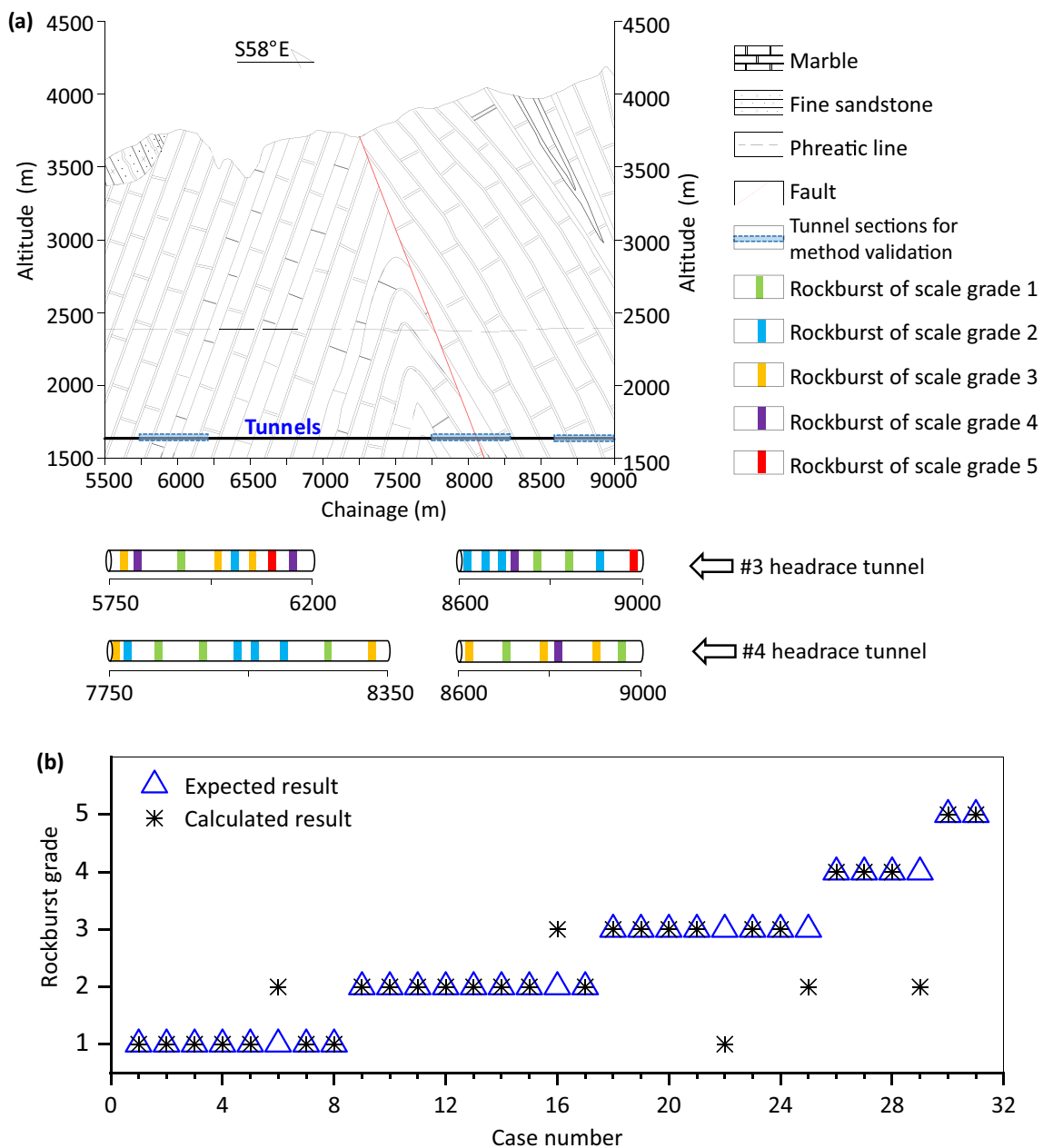


**Fig. 18** Results of the engineering validation analysis of the proposed method: **a** geological profile along the related tunnels and distribution of the validation cases and **b** comparison between the estimated result and actual rockburst scale for validation cases

results of rockburst intensities are as follows:  $P_{\text{none}} = 7.4\%$ ,  $P_{\text{slight}} = 11.4\%$ ,  $P_{\text{moderate}} = 7.9\%$ , and  $P_{\text{intensive}} = 73.3\%$ . Moreover, the output that was calculated by the ANN model of the rockburst scale was [0, 0, 0, 0, 1]. Based on both results, an intensive rockburst of grade 5 would occur on Nov. 11, 2011, or later. An in situ investigation showed that the rockburst that occurred on Nov. 11 was an intensive rockburst, and the rockburst pit was almost 40 m in length along the tunnel axis and reached a maximum height of 7 m and a maximum failure depth of approximately 1.2 m, as

shown in Fig. 19b. The volume of this rockburst pit was approximately 60 m<sup>3</sup> and graded as 5. The actual situations matched the warning and estimation results.

Thus, two rockbursts that have the same intensity may cause variable scales of damage (in volume) to the surrounding rock. Based on the estimation of the rockburst scale, it is possible to identify the characteristic differences of rockbursts that are of the same intensity from the other aspect and to provide useful details regarding potential rockbursts besides the intensity.

**Table 6** Microseismicity in the rockburst estimating volume by 24:00 on Nov. 20, 2011

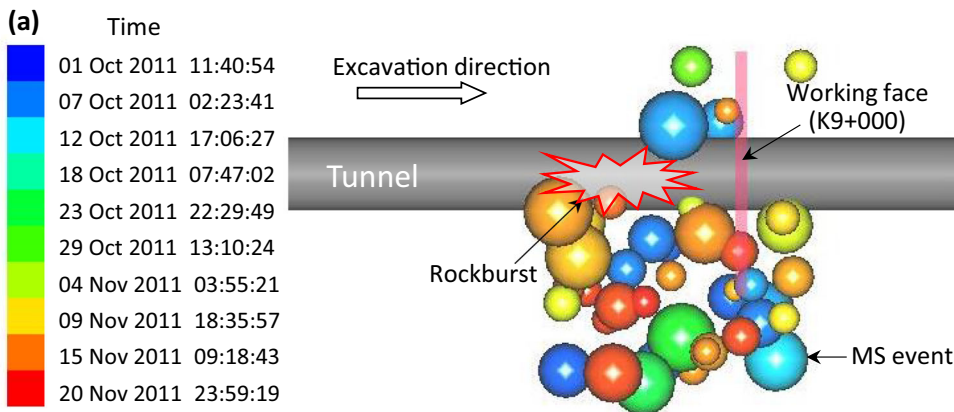
	Microseismic parameters					
	$N$	$E (\times 10^6 \text{J})$	$V (\times 10^4 \text{m}^3)$	$\dot{N}$	$\dot{E} (\times 10^4 \text{J})$	$\dot{V} (\times 10^3 \text{m}^3)$
Value	49	1.426	8.760	1.0	2.909	1.788

**Determination of the rockburst scale**

In the study, the volume of the rockburst pit ( $R_v$ ) is proposed as a new indicator of the failure scale of a rockburst.  $R_v$  is a superior indicator to the failure depth for evaluating the severity of a rockburst, while it is not easy to obtain. In this study, the scale data for most rockburst cases were approximated via mathematical calculation by establishing a rapid geometric model according to the geometrical shape of the rockburst pit. Field investigations in the Jinping tunnels showed that the rockburst pits could be characterized by regular geometric profiles in various cases. Feng et al. (2013) classified the profiles of common pits of rockbursts from the Jinping tunnels

into two types: nest-shaped and V-shaped, as presented in the examples in Fig. 20a–e. According to relevant studies, the rockburst pits can be characterized by nest-shaped, V-shaped (also called triangle-shaped), and bowl-shaped (in a few cases) geometric profiles (Ewy and Cook 1990; Xu et al. 2002; Gu et al. 2002). Therefore, an approximate geometrical model that corresponds to each type of rockburst shape can be constructed, and a simplified mathematical solution can be obtained for the calculation of the rockburst scale. When using this method, several aspects should be considered: (1) The simplified geometrical model may have different forms since it also depends on the profile of the rockburst pit along the axial direction of a tunnel, for both the vault shape and the V shape. (2)

**Fig. 19** Rockburst estimation results when the working face advanced to chainage 3#K9+000: **a** spatial distribution of the MS activity by 24:00 on Nov. 20 and **b** the rockburst that occurred in the north sidewall from chainage 3#K8+950 to 3#K8+990 on Nov. 21, 2011





For various unavoidable cases of irregular rockburst pits, the analysis should be conducted according to the circumstances. Geometrical simplification can still be used to calculate the scope of the rockburst scale (the upper and lower limits) by adopting regular models such as nest-shaped, V-shaped, and even rectangle-shaped models. The types of rockburst pits that are shown in Fig. 20f could be partitioned for calculation more than once and measured by an accumulative result. (3) This calculation method requires data on the length, depth, and height that are measured from multiple positions of the rockburst pit. The more available the data is, the more accurate the obtained result is. (4) Although this simplified mathematical method can provide only an approximate result regarding

the rockburst scale, it is sufficient for determining the grade of the rockburst scale, on which this study focuses.

The scale of a rockburst could also be approximated by measuring the volume of the rock mass ejected by the rockburst. This is a crude and relatively straightforward approach but is not easy to implement if the rock mass ejection by the rockburst are mixed with rocks that were abandoned during excavations. In addition, it may suffer from a few deficiencies if the ejected rocks have not been gathered well for disposal. In recent years, 3D laser scanning technology has been increasingly used in geotechnical engineering and underground projects. Obtaining 3D models with fine details as quick, precise, and untouched solutions for the reconstruction

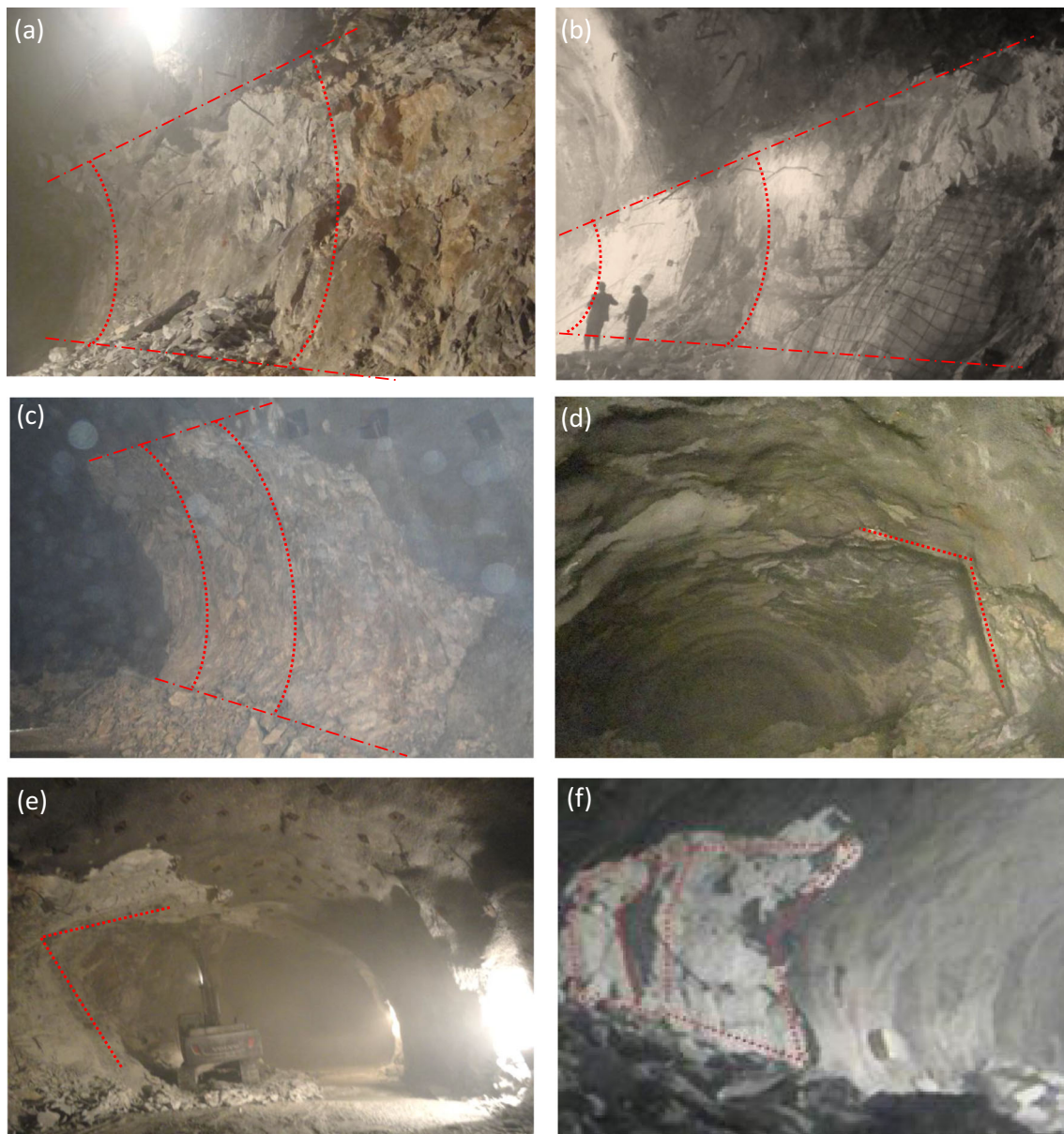


**Fig. 20** Examples of various types of rockburst pits on site. Herein, **a–c** are long nest-shaped rockbursts, **d–e** are V-shaped rockbursts, and **f** is a rockburst of irregular shape

of the surfaces of complex objects is convenient. If feasible, it is an effective solution via which the volume of a rockburst pit can be accurately identified.

In addition, this study is conducted based on a grading scheme of rockburst scale that is proposed in this paper. The accuracy of a rockburst prediction model depends on the grading scheme, which is a classification issue. The grading schemes may differ among views, which require further investigation.

## Conclusions

Compared with the previously proposed rockburst prediction methods, the potential rockburst scale, graded by the volume of the rockburst pit, is proposed as a new indicator in this study for analyzing the rockburst risk from a new perspective. Firstly, the principles for grading of the rockburst scale in the estimation method are discussed, and a grading scheme for the rockburst scale, composed of five grades, is established based on a statistical analysis of hundreds of rockburst cases. Then, the relationships between the MS parameters and the rockburst scale are extensively analyzed, and the results demonstrated that the average value for each MS parameter in the development process of the rockburst increases as the rockburst scale becomes bigger. Thirdly, a new microseismicity-based method that uses three MS parameters (the number of MS events, MS energy, and MS apparent volume) to obtain the potential failure scale of surrounding rock during rockburst risk estimation is presented, in which an ANN predictive model optimized by the GA is contained.

According to this proposed method, the rockburst occurrence and the grade of its potential scale can be early estimated in real time during tunnel excavation. Several advantages of the proposed method are identified: (a) a focused spatial rockburst estimating volume is used; (b) the precursory microseismicity in the spatial estimating volume could indicate the level of rockburst risk and provide important support for the early estimation of the rockburst scale; (c) the proposed ANN estimation model is easy to use and well understood, and the forms of input parameters and output results are simple; (d) and the estimation result and the proposed estimation model can be constantly updated.

The proposed estimation model has been trained on hundreds of typical rockburst cases that were collected from the tunnels at depths of 1900–2525 m in the Jinping II hydropower station in China. The engineering validation are carried out in the 1.85-km-long tunnel sections with continuous MS monitoring, and the result indicates that

approximately 83.9% of rockburst cases could be reliably estimated, which proves the applicability of the proposed method.

**Nomenclatures**  $R_v$ , the volume of the rockburst pit; MS, microseismic;  $N$ , cumulative number of MS events;  $E$ , cumulative microseismic energy;  $V$ , cumulative microseismic apparent volume;  $\dot{N}$ , microseismic event rate;  $\dot{E}$ , microseismic energy rate;  $\dot{V}$ , microseismic apparent volume rate; UCS, uniaxial compression strength; TS, tensile strength; ANN, artificial neural network; GA, genetic algorithm; BPNN, back-propagation neural network;  $W_{ij}$ , connective weight between neuron  $i$  and neuron  $j$ ;  $\theta_i$ , the neural network threshold; G-1, the rockburst of scale grade 1; G-2, the rockburst of scale grade 2; G-3, the rockburst of scale grade 3; G-4, the rockburst of scale grade 4; G-5, the rockburst of scale grade 5;  $x_{kj}$ , value of microseismic parameter  $j$  of the  $K$ th case;  $x_{Lj}$ , value of microseismic parameter  $j$  of the  $L$ th case;  $X_{ij}^*$ , normalization value of microseismic parameter  $j$  of case  $i$ ;  $X_{ij}$ , value of microseismic parameter  $j$  of sample  $i$ ;  $X_{j, \max}$ , the maximum value of microseismic parameter  $j$  among total cases;  $X_{j, \min}$ , the minimum value of microseismic parameter  $j$  among total cases;  $u_i$ , the result calculated by the artificial neural model for the  $i$ th learning sample;  $u_i^*$ , expected result for the  $i$ th learning sample;  $P_i$ , the probability of rockburst intensity  $i$ ;  $w_j$ , weighting coefficient of microseismic parameter  $j$  for rockburst warning;  $P_{ji}$ , functional relationship between parameter  $j$  and rockburst intensity  $i$

**Acknowledgements** The authors are grateful for the financial supports from the Basic Research Program of Natural Science from Shaanxi Science and Technology Department (Grant No. 2019JQ-171), the National Natural Science Foundation of China (Grant No. U1965205), and the Fundamental Research Funds for the Central Universities (Grant No. 300102210110). The microseismic monitoring data involved in this paper is obtained from the institute of Rock and Soil Mechanics, Chinese Academy of Sciences. The authors would also express their sincere thanks to Professors Shi-Yong Wu and Ya-Xun Xiao, as well as Dr. Hua-Jun Ming who gave support and assistance during microseismicity monitoring in Jinping II hydropower station project.

## References

- Abbas M, Morteza B (2010) Evolving neural network using a genetic algorithm for predicting the deformation modulus of rock masses. *Int J Rock Mech Min Sci* 47:246–253
- Adoko AC, Gokceoglu C, Wu L, Zuo QJ (2013) Knowledge-based and data-driven fuzzy modeling for rockburst prediction. *Int J Rock Mech Min Sci* 61(4):86–95
- Aswegen GA, Bulter AG (1993) Applications of quantitative seismology in South African gold mines. In: *Proceedings of 3rd international symposium on rock-bursts and seismicity in mines*. 16–18 August Canada, pp 261–266
- Cai M, Kaiser PK, Martin CD (2001) Quantification of rock mass damage in underground excavations from microseismic event monitoring. *Int J Rock Mech Min Sci* 38(8):1135–1145
- Chen BR, Feng XT, Ming HJ, Zhou H, Zeng XH, Feng GL, Xiao YX (2012) Evolution law and mechanism of rockburst in deep tunnel: time delayed rockburst. *Chin J Rock Mech Eng* 31(3):561–569 (in chinese)

- Chen DF, Feng XT, Xu DP, Jiang Q, Yang CX, Yao PP (2016) Use of an improved ANN model to predict collapse depth of thin and extremely thin layered rock strata during tunnelling. *Tunn Undergr Space Technol* 51:372–386
- Chinese standards, GB 50287-2016 (2016) Specification for geological survey of hydropower engineering. China planning press, Beijing
- Chinese Standards, NB/T 10143–2019 (2019) Technical code for rockburst risk assessment of hydropower projects. China Water&Power Press, Beijing
- Cooper GF, Herskovits E (1992) A Bayesian method for the induction of probabilistic networks from data. *Mach Learn* 9(4):309–347
- Das R, Singh PK, Kainthola A, Panthee S, Singh TN (2017) Numerical analysis of surface subsidence in asymmetric parallel highway tunnels. *J Rock Mech Geotech Eng* 9(1):170–179
- Deng JL (1982) Control problems of grey systems. *Syst Control Lett* 1(5):2–7
- Delen D, Walker G, Kadam A (2005) Predicting breast cancer survivability: a comparison of three data mining methods. *Artif Intell Med* 34(2):113–127
- Dubois D, Prade H (1980) Fuzzy sets and systems: theory and applications. Academic Press, Utah
- Everitt BS, Landau S, Leese M (2001) Cluster analysis. Oxford University Press, New York
- Ewy RT, Cook NGW (1990) Deformation and fracture around cylindrical openings in rock—II. Initiation, growth and interaction of fractures. *Int J Rock Mech Min Sci* 27(5):409–427
- Feng XT (2017) Rockburst: mechanisms, monitoring, warning and mitigation. Butterworth-Heinemann, Oxford
- Feng XT, Hudson JA (2011) Rock engineering and design. CRC Pres/Balkema, Leiden
- Feng XT, Chen BR, Li SJ, Zhang CQ, Xiao YX, Feng GL, Zhou H, Qiu SL, Zhao ZN, Yu Y, Chen DF, Ming HJ (2012) Studies on the evolution process of rockbursts in deep tunnels. *J Rock Mech Geotech Eng* 4(4):289–295
- Feng XT, Chen BR, Zhang CQ, Li SJ, Wu SY (2013) Mechanism, warning and dynamic control of rockburst development processes. Science Press, Beijing (in Chinese)
- Feng GL, Feng XT, Chen BR, Xiao YX, Jiang Q (2015a) Sectional velocity model for microseismic source location in tunnels. *Tunn Undergr Space Technol* 45:73–83
- Feng GL, Feng XT, Chen BR, Xiao YX, Yu Y (2015b) A microseismic method for dynamic warning of rockburst development processes in tunnels. *Rock Mech Rock Eng* 48(5):2061–2076
- Feng GL, Feng XT, Chen BR, Xiao YX, Liu GF, Zhang W, Hu L (2020) Characteristics of microseismicity during breakthrough in deep tunnels: case study of Jinping-II hydropower station in China. *Int J Geomech* 20(2):04019163
- Gallagher MR, Downs T (2003) Visualization of learning in multilayer perceptron networks using principal component analysis. *IEEE Trans Syst Man Cybern B Cybern* 33(1):28–34
- Goldberg DE (1989) Genetic algorithms in search, optimization, and machine learning. Addison-Wesley publishing company, Massachusetts
- Gong FQ, Si XF, Li XB, Wang SY (2019) Experimental investigation of strain Rockburst in circular caverns under deep three-dimensional high-stress conditions. *Rock Mech Rock Eng* 52(5):1459–1474
- Gu MC, He FL, Chen CZ (2002) Study on rockburst in Qingling Tunnel. *Chin J Rock Mech Eng* 21(9):1324–1329
- Hoek E, Marinos P, Benissi M (1998) Applicability of the geological strength index (GSI) classification for very weak and sheared rock masses: the case of Athens Schist Formation. *Bull Eng Geol Environ* 57:151–160
- Hu L, Feng XT, Xiao YX, Wang R, Feng GL, Zb Y, Niu WJ, Zhang W (2019) Effects of structural planes on rockburst position with respect to tunnel cross-sections: a case study involving a railway tunnel in China. *Bull Eng Geol Environ*. <https://doi.org/10.1007/s10064-019-01593-0>
- Itasca (2012) FLAC3D Manual: Fast Lagrangian Analysis of Continua in 3 dimensions-Version 5.0, Itasca Consulting Group, Inc., Minnesota
- Jiang Q, Feng XT, Xiang TB, Su GS (2010) Rockburst characteristics and numerical simulation based on a new energy index: a case study of a tunnel at 2,500 m depth. *Bull Eng Geol Environ* 69(3):381–388
- Kaiser PK, Tannant DD, McCreath DR (1996) Canadian rockburst support handbook. Geomechanics Research Centre/Laurentian University, Sudbury
- Kavzoglu T, Mather PM (2000) Using feature selection techniques to produce smaller neural networks with better generalisation capabilities. *Geosci Remote Sens Symp* 7:3069–3071
- Li A, Dai F, Liu Y, Du HB, Jiang RC (2021) Dynamic stability evaluation of underground cavern sidewalls against flexural toppling considering excavation-induced damage. *Tunn Undergr Space Technol* 111:103903
- Liu GF, Feng XT, Feng GL, Chen BR, Chen DF, Duan SQ (2016) A method for dynamic risk assessment and management of rockbursts in drill and blast tunnel. *Rock Mech Rock Eng* 49(8):3257–3279
- Ma TH, Tang CA, Tang LX, Zhang WD, Wang LR (2015) Rockburst characteristics and microseismic monitoring of deep-buried tunnels for Jinping II hydropower station. *Tunn Undergr Space Tech* 49:345–368
- McCreary R, Mcgaughey J, Potvin Y, Ecobichon D, Hudyma M, Kanduth H (1992) Results from MS monitoring, conventional instrumentation, and tomography surveys in the creation and thinning of a burst-prone still pillar. *Pure Appl Geophys* 139(3):349–373
- Mendecki AJ (1996) Seismic monitoring in mines. Chapman & Hall, London
- Ortlepp WD, Stacey TR (1994) Rockburst mechanisms in tunnels and shafts. *Tunn Undergr Sp Tech* 9(1):59–65
- Rayburn DB, Klimauskas CC (1990) The use of back propagation neural networks to identify mediator-specific cardiovascular waveforms. *Int. Joint Conf. Neural Netw* 2:105–110
- Sen S, Sezer EA, Gokceoglu C, Yagiz S (2012) On sampling strategies for small and continuous data with the modeling of genetic programming and adaptive neuro-fuzzy inference system. *J Intell Fuzzy Syst* 23(6):297–304
- Sezer EA, Nefeslioglu HA, Gokceoglu C (2014) An assessment on producing synthetic samples by fuzzy C-means for limited number of data in prediction models. *Appl Soft Comput* 24:126–134
- Shan ZG, Yan P (2010) Management of rock bursts during excavation of the deep tunnels in Jinping II hydropower station. *Bull Eng Geol Environ* 69:353–363
- Sietsma J, Dow RJF (1999) Back propagation networks that generalize. *Neural Netw* 12:65–69
- Simpson PK (1990) Artificial neural system. Pergamon Press, New York
- Suchatvee S, Herbert HE (2006) Artificial neural networks for predicting the maximum surface settlement caused by EPB shield tunnelling. *Tunn Undergr Sp Technol* 21:133–115
- Tang CA, Wang JM, Zhang JJ (2010) Preliminary engineering application of microseismic monitoring technique to rockburst prediction in tunnelling of Jinping II project. *J Rock Mech Geotech Eng* 2(3):193–208
- Vapnik VN (1995) The nature of statistical learning theory. Springer, New York
- Wang XT, Li SC, Xu ZH, Xue YG, Hu J, Li ZQ, Zhang B (2019) An interval fuzzy comprehensive assessment method for rock burst in



- underground caverns and its engineering application. *Bull Eng Geol Environ* 78:5161–5176
- Xu LS, Wang LS, Li YL (2002) Study on mechanism and judgement of rockbursts. *Rock Soil Mech* 23(3):300–303 (in Chinese)
- Xu NW, Li TB, Dai F (2016) Microseismic monitoring of strainburst activities in deep tunnels at the Jinping II hydropower station, China. *Rock Mech Rock Eng* 49(3):981–1000
- Yu Y, Chen BR, Xu CJ, Diao XH (2016) Analysis for microseismic energy of immediate rockbursts in deep tunnels with different excavation methods. *Int J Geomech* 17(5):04016119
- Zhang CQ, Feng XT, Zhou H, Qiu SL, Wu WP (2013) Rockmass damage development following two extremely intense rockbursts in deep tunnels at Jinping II hydropower station, southwestern China. *Bull Eng Geol Environ* 72:237–247
- Zhang H, Chen L, Chen SG, Sun JC, Yang JS (2018) The spatiotemporal distribution law of microseismic events and rockburst characteristics of the deeply buried tunnel group. *Energies* 11(12):3257
- Zhou J, Li XB, Shi XZ (2012) Long-term prediction model of rockburst in underground openings using heuristic algorithms and support vector machines. *Saf Sci* 50(4):629–644
- Zhou J, Li XB, Mitri HS (2015) Comparative performance of six supervised learning methods for the development of models of hard rock pillar stability prediction. *Nat Hazards* 79(1):291–316